Cellular Physiology and Biochemistry

Cell Physiol Biochem 2015;35:1499-1526
DOI: 10.1159/000369710
Published online: March 12, 2015
Accepted: November 24, 2014





1421-9778/15/0354-1499$39.50/0



**Original Paper**

# Synergistic Anticancer Potential of Dichloroacetate and Estradiol Analogue Exerting their Effect via ROS-JNK-Bcl-2-Mediated Signalling Pathways

Xiao Xing Stander  Barend André Stander  Annie Margaretha Joubert

Department of Physiology, School of Medicine, Faculty of Health Sciences, University of Pretoria, Pretoria, Gauteng, South Africa

**Key Words**
Combination treatment • Antimitotic • DCA • MCF-7 • MCF-12A • Apoptosis • Autophagy • JNK • Bcl-2 and ROS

**Abstract**
***Background:*** C9, a newly *in silico*-designed inhibitor of microtubule dynamics induces $G_2$/M arrest culminating in apoptosis. Dichloroacetate (DCA) inhibits pyruvate dehydrogenase kinase, an enzyme that promotes pyruvate entry into mitochondria. The use of antitumor drugs targeting different cancer features can be a more effective way to overcome drug resistance. ***Methods:*** The influence of C9 (130 nM) + DCA (7.5 mM) on MCF-7 and MCF-12 cells was assessed via microscopy, spectrophotometry, global gene expression and flow cytometry assays. ***Results:*** An LDH assay showed that C9+DCA treatment decreased cell viability to 83.5% in MCF-7 cells when compared to the non-tumorigenic MCF-12A cells 92.4% ($P < 0.05$). C9- and C9+DCA treatment induced mitochondrial membrane potential depolarization in MCF-7 cells but not in MCF-12A cells ($P < 0.05$). The occurrence of apoptosis was associated with increased hypo- and hyper-phosphorylation of Bcl-2 $Ser^{70}$ and caspase 7 activation. Kinase inhibition revealed sustained activation of the JNK pathway caused increased Bcl-2 protein $Ser^{70}$ hypo-and hyper-phosphorylation. Elevated levels of DCF fluorescence was observed in DCA-, C9- and C9+DCA-exposed MCF-7 cells, but not in MCF-12A cells, indicating cytosolic $H_2O_2/Fe^{2+}$ formation in treated tumorigenic cells. LC3-II expression was elevated in C9+DCA-treated cells in both cell lines, indicating that autophagy was also induced. ***Conclusions:*** Synergistic effects of C9+DCA were demonstrated on breast carcinoma and non-tumorigenic cells with selectivity towards the MCF-7 cells. Antimitotic compound C9 in combination with a glycolytic inhibitor dichloroacetate eradicates breast cancer cells through ROS-JNK-Bcl-2-mediated signalling pathways *in vitro* and it is argued that autophagy acts as protective mechanism in the treated cells before apoptosis occurs.



Xiao Xing Stander

Department of Physiology, School of Medicine, Faculty of Health Sciences, University of Pretoria, Private Bag X323, Arcadia, Pretoria 0007, Gauteng, South Africa
Tel. +27 12 420 2864, Fax +27 86 651 5929, E-mail xiaoxing.stander@up.ac.za

## Introduction

Increased understanding of the evolutionary origins of cancer has helped researchers comprehend how resistance to anticancer treatment emerges [1]. Hanahan and Weinberg identified six hallmarks of cancer in 2000 [2] and four additional characterises in 2011 [3]. These ten hallmarks include eight acquired features and two enabling features. The eight acquired features are self-sufficiency in growth signals, insensitivity to anti-growth signals, evading cell death, limitless replicative potential, sustained angiogenesis, evasion of the immune system, deregulated metabolism and tissue invasion, and metastasis. Unstable genomes and tumour-promoting inflammation are the two enabling features [3]. Treatment of cancer with combination therapies targeting at least two different pathways is preferable [4]. This can be achieved by treating cancer with different types of chemotherapeutic agents or one agent that is capable of targeting numerous signalling pathways.

Antimitotic compounds are capable of targeting hallmarks of cancer that promote a hyperproliferative phenotype. Bioenergetic alterations in cancers including a pro-oxidant status, increased glycolysis and inhibited mitochondrial oxidative phosphorylation (OXPHOS), aid in increased proliferation and insensitivity to pro-apoptotic signals [3, 5]. These characteristics separate cancer cells from normal functioning cells and can be seen as a weak point and a target for selective growth inhibition [1]. The combination of antimitotic compounds together with compounds that can target the dysregulated metabolism of many cancers provide a means to target more hallmarks of cancer and has the potential to be more selective towards killing cancer cells.

The combination of the antimitotic compound doxirubicin with 2-deoxy-D-glucose (2-DG), a compound that targets the dysregulated metabolism of many cancers and that recently passed a phase I clinical trial and phase II studies in several solid tumours, has demonstrated therapeutic promise in patients with advanced solid tumors [6]. Tagg et al. [7] demonstrated that the combination of a sulphamoylated 2-methoxyestradiol (2ME) analogue and 2-DG was potent against breast- and prostate cancers *in vivo*.

C9 is another sulphamoylated analogue of 2ME and was *in silico* designed by our group [8-10]. C9 has improved bioavailability because of the ability of the sulphamoyl moiety to reversibly bind to carbonic anhydrase II present in erythrocytes and, in turn, this allows C9 to circumvent liver metabolism [11]. 2-Ethoxy group at carbon position two of C9 is known to improve the antimitotic activity of estradiol analogues [12] and dehydration at positions 14 and 15 was shown to have increased antiproliferative and anticancer activities [13]. Dichloroacetate (DCA), a small two-carbon molecule that targets cancer cell metabolisms was also investigated. DCA and Nov3r-class agents are well-characterised inhibitors of pyruvate dehydrogenase kinase (PDK) [14].

Recent studies suggest that forcing cells into oxidative phosphorylation suppresses cancer growth [15-17]. The increased pyruvate dehydrogenase (PDH) activity shifts metabolism from glycolysis to oxidative phosphorylation and decreases mitochondrial membrane potential hyperpolarization, which opens mitochondrial transition pores [18]. This allows for the translocation of reactive oxygen species (ROS) from the mitochondrial matrix to the cytoplasm and increases ROS-signalling, as well as restoring normal metabolism, thereby decreasing lactate production in metabolically altered cells [18, 19].

In a 2007 study DCA reduced mitochondrial membrane potential, caused the formation of ROS and also caused the release of the pro-apoptotic effector cytochrome *c* in non-small-cell lung cancer (A549), glioblastoma (M059K), and breast cancer cells (MCF-7), but not normal cells [18]. Michelakis et al. utilised DCA to treat glioblastoma patients for 15 months and reported that this small molecule has the ability to induce apoptosis *in vitro* and *in vivo* [20]. Sutendra et al. demonstrated that DCA re-activates mitochondrial metabolism in cancer cells (*in vitro*, xenotransplant model and *in vivo*) through signalling that involves the inhibition of PDK. They showed the mitochondria-targeting metabolic modulators that increase PDH activity suppress angiogenesis as well, normalizing the pseudo-hypoxic hypoxia-inducible factor 1 (HIF1α) signals in solid tumors [21]. Currently, DCA is being used in clinical trials

for the treatment of brain tumours, breast cancer and lung cancer (clinicaltrials.gov) [22].

DCA and C9 are two compounds with different anticancer activities, one being a glycolytic inhibitor and other one an antimitotic compound. C9 is an antimitotic compound which disrupts tubulin polymerization in actively dividing cells. Treatment of C9 on cells resulted $G_2$/M phase cell cycle arrest and apoptotic cell death [8, 9]. DCA is known to induce ROS level and intrinsic apoptotic cell death by forcing cancer cells to utilize the mitochondria for energy production [18, 21]. It is thus possible that combination treatment of cells with DCA and C9 may induce apoptosis via ROS-mediated pathway. There is currently no literature to elucidate the mechanisms of action of *in silico*-designed C9 and DCA for the treatment of cancer.

Our group previously demonstrated the synergistic effects of 130 nM C9 combined with 7.5 mM DCA on breast carcinoma MCF-7, and non-tumorigenic MCF-12A cells with selectivity towards the breast carcinoma cells [9]. The Chou-Talalay method combination index (CI) for multiple drug effect interactions introduced the concept for quantitative definition of synergism [23]. The combination index of 0.88 indicates synergistic effects of the compounds (C9 [130 nM] / C9 [160 nM] + DCA [7.5 mM] / DCA [150 mM]) for 24 h treatment and it was calculated according to a mathematical formula described previously [23-25]. In the pilot study, apoptosis was identified as one of the mechanisms that lead to C9+DCA-mediated cell death. It was proposed that the selectivity of the combination treatment is associated with the DCA-mediated restoration of oxidative phosphorylation in MCF-7 cells, which, in turn, contributes to reactive oxygen species formation, mitochondrial permeabilisation and ultimately, culminating in apoptosis. In the present study we investigated the link between reactive oxygen species signalling, mitochondrial membrane depolarisation, c-Jun N-terminal kinases (JNK) signalling and B-cell lymphoma 2 (Bcl-2) phosphorylation and apoptotic cell death in order to further elucidate the mechanism of action of C9+DCA on breast cells.

## Materials and Methods

*Compounds and reagents*

Compound 2-ethyl-3-*O*-sulphamoyl-estra-1,3,5(10),15-tetraen-3-ol-17-one (C9 or ESE-15-one) was synthesized by iThemba Pharmaceuticals (Pty) Ltd. (Modderfontein, Midrand, RSA). DCA (powder) was purchased from Sigma Chemical Co. (St. Louis, MO, USA). The concentration of combination treatment tested were 130 nM C9 combined with 7.5 mM DCA.

Gibco® Dulbecco's Modified Eagle's Medium (DMEM) and Ham's F-12 Nutrient Mixture (F-12) were purchased from Life Technologies ™ South Africa (Pty) Ltd. (Fairland, RSA). Bouin's fixative, 2′, 7′-dichlorodihydrofluorescein diacetate ($H_2$DCF-DA), ferric iron chelator deferoxamine mesylate salt (DFO), antioxidant *N*-acetyl-*L*-cysteine (NAC), JNK inhibitor (JNKi) SP600125 and p38α inhibitor (p38i) SB239063 were supplied by Sigma Aldrich (St. Louis, MO, USA). Heat-inactivated fetal bovine serum (FBS) (PAA Laboratories (Pty) Ltd. Morningside, QLD, AUS), sterile cell culture flasks and plates (96-well plates and 6-well plates) were obtained through Separations (Pty) Ltd. (Randburg, Johannesburg, RSA). Phosphate-buffered saline (PBS) was purchased from Gibco BRL (Invitrogen, Carlsbad, California, USA). Trypsin/Versene (0.125% trypsin, 0.1 Versene EDTA), penicillin, streptomycin and fungizone were purchased from Highveld Biological (Pty) Ltd. (Sandringham, Johannesburg, RSA). Haematoxylin, eosin, ethanol, xylol, Entellam® fixative cholera toxin, glutaraldehyde and triton X-100 were purchased from Merck (Munich, Germany).

The Lactate Dehydrogenase Cytotoxicity Assay Kit from BioVision Inc. (Mountain View, California, USA), the primary monoclonal mouse anti-tubulin alpha antibody from IMGENE (Alexandria, VA, USA) (cat no. IMG-80196), the rabbit antibody for anti-active caspase 7 from BioVision Inc. (Mountain View, California, USA) and a secondary anti-rabbit antibody conjugated to Dylight™ 488 from Rockland Inc (Gilbertsville, Pennsylvania, USA) were purchased through BIOCOM biotech (Pty) Ltd. (Pretoria, Gauteng, RSA). Fluorescein-isothiocyanate (FITC)-conjugated anti-autophagy-related (LC3) antibody (NB600-1384) was purchased from Novus Biologicals Ltd. (Cambridge, UK). MitoCapture™ Apoptosis Detection Kit [K250-

25] was purchased from BioVision (Mountain View, California, USA). FlowCellect™ Bcl-2 Activation Dual Detection Kit produced by Millipore Corporation (Billerica, MA, USA) was purchased through Microsep (Pty) Ltd (Johannesburg, Gauteng, RSA). The fluorophore-labelled donkey anti-mouse heavy and light chain secondary IgG with Alexa Fluor 350 secondary antibody from Invitrogen (Carlsbad, California, USA) was purchased from The Scientific Group (Johannesburg, RSA). Qiagen® RNeasy Plant Mini Kit and RNase-free DNase were purchased from Southern Cross Biotechnology (Pty) Ltd. (Cape Town, RSA). Agilent's and 44k 60-mer human oligo slides, Low RNA Input Fluorescent Linear Amplification Kit, 2x GEx Hybridisation Buffer HI-RPM, Gene Expression (GE) Wash Buffer 1 and 2, Stabilisation and Drying Solution were obtained from Agilent Technologies (Pty) Ltd. (Palo Alto, California, USA). Cy-3 and Cy-5 fluorescent dyes were supplied by Amersham Biosciences (Pittsburgh, USA).

*Cell cultures*

The breast adenocarcinoma tumorigenic MCF-7 (estrogen receptor negative) and non-tumorigenic breast epithelial cells MCF-12A cell line (estrogen receptor negative) were obtained from the American Type Culture Collection (ATCC, Manassas, Virginia, USA). MCF-7 cells were cultured in DMEM and supplemented with 10% heat-inactivated fetal bovine serum (FBS), 1% penicillin G (100 U/ml), streptomycin (100 µg/ml) and fungizone (250 µg/l). MCF-12A cells were cultured in a 1:1 mixture of DMEM and Ham's F12 medium completed with epidermal growth factor (20 ng/ml), cholera toxin (100 ng/ml), insulin (0.01 mg/ml), hydrocortisone (500 ng/ml), 10% heat-inactivated FCS, 1% penicillin G (100 U/ml), streptomycin (100 µg/ml) and fungizone (250 µg/l). All cells were grown at 37°C in a humidified atmosphere containing 5% $CO_2$.

*Cell viability*

Lactate dehydrogenase (LDH) is present in all cell types and is rapidly released into the cell culture medium upon damage of the plasma membrane [26]. The Lactate Dehydrogenase Cytotoxicity Assay Kit from BioVision Inc. (Mountain View, California, USA) was used to determine the effects of compounds (130 nM C9, 7.5 mM DCA and C9+DCA) on MCF-7 and MCF-12A after 24 h. The cell viability was tested according to manufacturer's instructions. Briefly, cells were seeded at densities of 5000 cells per well in 96-well microtiter plates and cultured for 24 h. After various treatments for 24 h, cells were centrifuged for 1 min and 10 µl of medium/well was transferred to a plate contain LDH Reaction Mix solution (100 µl/well). Plates were allowed to develop colour for 60 min and the absorbance were determined spectrophotometrically at 450 nm with an ELX800 Universal Microplate Reader (Bio-Tek Instruments Inc., Vermont, USA).

*Cell morphology via light microscopy*

Haematoxylin and eosin (H&E) stains were used to recognise various cytoplasmic and nuclear morphologic changes [27], as well as to determine the mitotic index [28]. MCF-7 and MCF-12A cells were seeded in 6-well plates at a density of 375 000 cells/3 ml medium/well on heat-sterilized cover slips. Cells were exposed to compounds compounds (130 nM C9, 7.5 mM DCA and C9+DCA) and appropriate controls for 24 h. Prior to staining, cover slips were transferred and fixed with Bouin's fixative for 30 min. Mayer's haemalum was added and samples were left for 20 min before they were rinsed with tap water and ethanol (70%). Subsequently, 1% eosin was used to stain the cells for 5 min. Cover slips were rinsed twice with 70%, 96% and 100% ethanol and then xylol to ensure that excess water was removed. Samples were left to dry and observed under a Zeiss Axiovert MRs microscope (Carl Zeiss MicroImaging GmbH, Göttingen, Germany). In this experiment, data captured consists of qualitative image examination, as well as quantitative mitotic indices. The latter was acquired by analysing and counting mitosis phase (prophase, metaphase, anaphase and telophase) of 1 000 cells per slide [29].

*Confocal microscopy Immunofluorescent detection of tubulin architecture*

Confocal microscopy was employed to detect the effect of C9 (130 nM), DCA (7.5 mM) and C9+DCA (7.5 mM) on tubulin architecture of MCF-7 and MCF-12A cells. Cells were cultured in 6-well plates on cover slips and exposed to compounds (130 nM C9, 7.5 mM DCA and C9+DCA) for 24 h respectively. Cells were washed with cytoskeletal buffer (CB) (60 mM 1,4 piperazinediethanesulfonic acid, 27 mM 4-(2-hydroxyethyl)-1-piperazineethanesulfonic acid, 10 mM ethylene glycol tetraacetic acid, 4 mM magnesium sulphate heptahydrate, pH = 7.0) and fixated with 0.3% glutaraldehyde at 37°C for 10 min. Subsequently, 6-well plates were placed onto a rotating orbital shaker at 5 revolutions/min. Cellular membranes were permeabilised

with 1% triton X-100. Unreacted aldehydes were removed with a reducing agent solution prepared by dissolving highly toxic sodium borohydride in PBS (1 mg/ml). Cells were washed with PBS and blocked in 5% bovine serum albumin (BSA) for 60 min at room temperature. Mouse monoclonal anti-α-tubulin antibody (IMG-80196, Imgenex) was used for microtubule structure detection (1:100 for 1.5 h). Cells were counter-stained with fluorophore-labelled donkey anti-mouse heavy and light chain secondary IgG with Alexa Fluor 350 (Invitrogen) fluorescent probe (1:125 for 1 h). Nuclei were stained with 4',6-diamidino-2-phenylindole (DAPI, Sigma) afterwards for 10 min. Stained cells were mounted on microscopy slides and viewed with a Zeiss 510 META confocal laser microscope (Carl Zeiss MicroImaging GmbH, Göttingen, Germany) [30].

*Microarray gene expression analysis*

Gene expression changes induced by the combination exposure of C9 and DCA on MCF-7 and MCF-12A cells were analysed using microarray technology. Agilent's Human 1A Oligo 60-mer Microarray (V2) 44k slides (Agilent Technologies (Pty) Ltd. (Palo Alto, CA, USA)) were used to collect genomic information from C9 in combination with DCA-treated- and vehicle-exposed MCF-7 and MCF-12A cells respectively. Agilent 44K slides represent 60-mer oligonucleotide probes that span conserved exons and are designed to represent genes in the human genome (~41,000 human genes and transcripts) across the transcripts of the targeted full length genes. Three biological replicates were used in a microarray experiment and a dye-swop methodology within one biological replicate was incorporated in the experimental design in order to remove the effects of dye-bias on statistical analyses.

Exponentially growing MCF-12A and MCF-7 cells were seeded at 750 000 cells/25cm$^2$ flasks. After 24 h of attachment, medium was discarded and cells were exposed to C9+DCA and incubated for 24 h. After exposure, total RNA was isolated from vehicle- and C9+DCA-exposed MCF-7 and MCF-12A cells using Qiagen Plant Mini Kit columns (as described previously by Stander *et al.* (2010) [31]. Pure total RNA was used for complimentary ribonucleic acid (cRNA) synthesis. Total RNA was suspended in RNase-free water (50 µl) and was quantified with the NanoDrop1000 (Thermo Fisher Scientific Inc. Wilmington, Delaware, USA) and tested for integrity by means of electrophoresis. RNA was considered completely intact when clear 28S and 18S rRNA bands, with a 28S:18S intensity ratio was approximately 2:1. Agilent's Low RNA Input Fluorescent Linear Amplification Kit was used to generate fluorescently labelled complimentary ribonucleic acid (cRNA). Labelled cRNA was suspended in 35 µl RNase-free water and was spectrophotometrically quantified with the NanoDrop 1000 (Thermo Fisher Scientific Inc. Wilmington, Delaware, USA). cRNA was considered pure of organic contamination (*e.g.* ethanol or phenol) with a 260/230 ratio greater than 1.5. Pure cRNA was hybridized to Agilent Human 1A (V2) oligonucleotide 44K microarray slides according to the manufactures guidelines using Agilent's 2x GEx Hybridization Buffer HI-RPM in Agilent's SureHyb chambers. The assembled slide chamber was placed in Agilent's hybridization oven set to 65˚C and 10 rpm. Samples were hybridized at for 17 hours. Afterwards the slides were washed twice for 1 min in Falcon tubes containing Agilent's Gene Expression Wash Buffer 1 at room temperature and once in Falcon tubes containing Agilent's Gene Expression Wash Buffer 2 at 37˚C for 1 min. The slides were transferred to acetonitrile for 1 min and then subsequently to Agilent's Stabilization and Drying Solution to help prevent ozone bleaching of the Cy-fluorochromes. The slides were gently removed from the Stabilization and Drying Solution and scanned immediately. Slides were scanned with the Axon Genepix 4000B Scanner (Molecular Devices Corporation, Sunnyvale, CA, USA) provided by the African Centre of Gene Technology (ACGT) Microarray Facility at the University of Pretoria. Spotfinding and statistical analysis after spotfinding were performed using Genepix Pro 6.1 (Molecular Devices Corporation, Sunnyvale, CA, USA) and Limma with the LimmaGUI interface [32, 33] respectively as described previously by Stander et al. [31].

The differentially expressed genes responsive to combination treatment in both cell lines were compared using GeneVenn [34] and 74 genes were found to be affected in both cell lines after 24 h exposure. Mapping of differentially expressed genes to biochemical pathways and Gene Ontology (GO) categories were performed by utilizing GeneCodis3 (3.0 versions) [35].

*Oxidative stress test*

The fluorescent compound 2', 7'-dichlorofluorescein (DCF) (DCF test) is used to evaluate intracellular oxidative stress [36]. Cells were cultured for 24 h and exposed compounds (130 nM C9, 7.5 mM DCA and C9+DCA) for 24 h. Subsequently, cells were trypsinized and incubated with 10 µM $H_2$DCF for 20 min.

Fluorescence of the compound DCF was measured with a FACS FC500 System flow cytometer (Beckman Coulter SA (Pty) Ltd.). Ferric iron chelator deferoxamine mesylate salt (DFO, 100 μM) and antioxidant *N*-acetyl-*L*-cysteine (NAC, 5mM) were used as positive controls in this experiment. Experimental data from at least three biological repeats for DCF test were statistically analysed with a Java-based flow cytometry data analysis program WEASEL v3.0.2 (trail version, available from Walter and Eliza Hall institute of Medical Research).

*Mitochondrial membrane potential depolarization*

The altered mitochondrial membrane potential were detected by MitoCapture™ apoptosis detection kit produced by BioVision Inc. (Mountain View, CA, USA) as described previously [10]. Cells were cultured for 24 h and were exposed to compounds compounds (130 nM C9, 7.5 mM DCA and C9+DCA) for 24 h respectively. Subsequently, cells were trypsinized and incubated with 1 ml of MitoCapture™ reagent for 15 min. At least 10 000 events with fluorescent dye were measured with a fluorescence activated cell sorting (FACS) FC500 System flow cytometer (Beckman Coulter SA (Pty) Ltd.). Experimental data from at least three biological repeats for mitochondrial membrane potential depolarization were statically analysed with non-commercialized Cyflogic software 1.2.1 (Pertu Therho, Turku, Finland).

*Bcl-2 expression and phosphorylation at Serine 70*

Flow cytometry was employed to study the overall expression and phosphorylation status of Bcl-2 at serine 70 in the treated MCF-7- and MCF-12A cell lines. In response to a variety of extracellular stimuli, Bcl-2 releases pro-apoptotic factors such as Bax, thereby diminishing its inhibitory action and enables Bax oligomerazation on the mitochondrial membrane [37]. Thus, Bcl-2 is an anti-apoptotic protein that plays a role in modulating the membrane potential of mitochondria. An intracellular increase in the expression of Bcl-2 protein is associated with its anti-apoptotic effects by preventing mitochondrial depolarization through its interaction and ultimate inhibition of Bax [38]. However, Bcl-2/Bax heterodimerization is not sufficient for full Bcl-2 anti-apoptotic function. Phosphorylation of Bcl-2 serine 70 ($Ser^{70}$) is a crucial requirement which complete its death suppressor signalling activity [39]. Dephosphorylation of Bcl-2 at $Ser^{70}$ is considered pro-apoptotic [38]. In contrast, phosphorylation of Bcl-2 at $Ser^{70}$ single-sited is anti-apoptotic, while multi-site phosphorylation at $Ser^{70}$, $Trp^{69}$ and $Ser^{87}$ is pro-apoptotic [40].

Merck Millipore's FlowCellect™ Bcl-2 Activation Dual Detection Kit was used for this purpose (detailed method previously described in Stander et al. [10]). The kit contains two antibodies that quantify the total amount of Bcl-2 protein (FL1 Log) and the S70 phosphorylation status of Bcl-2 per cell simultaneously (FL3 Log). The range of normal phosphorylation was regarded as 7.5-75 (FL3 Log). Cells that had an increase in FL3 fluorescence intensity of above 75 were considered to be cells that contained more phosphorylated serine 70 Bcl-2 proteins when compared to the control and regarded as hyper-phosphorylated pBcl-2. Conversely, cells that had an increase in FL3 fluorescence intensity of below 7.5 were considered to be cells that contained less phosphorylated serine 70 Bcl-2 proteins when compared to the control regarded as hypo-phosphorylated pBcl-2.

The oxidative stress level alteration may trigger cascade events, which result in the activation of p38 and JNK [41]. The JNK inhibitor (JNKi) SP600125 (20 μM) and p38α inhibitor (p38i) SB239063 (15 μM) were included in the experiment to test whether these pathways play a role with regard to activation/deactivation of Bcl-2 protein in MCF-7- and MCF-12A cells. Concentrations were chosen on the basis of literature [42].

*Caspase 7 activity*

A rabbit anti-active caspase 7 from BioVision Inc. (Mountain View, California, USA) and an anti-rabbit antibody conjugated to Dylight™ 488 from Rockland Inc (Gilbertsville, Pennsylvania, USA) were purchased from BIOCOM biotech (Pty) Ltd. (Pretoria, Gauteng, RSA) and were used to study protein expression changes of active/cleaved caspase 7 in the MCF-7- and MCF-12A cells after 24 h treatment with 130 nM C9-, 7.5 mM DCA- and C9+DCA respectively.

*Autophagic activity*

Flow cytometry was employed to quantify microtubule-associated protein 1A/1B-light chain 3 (LC3) -phosphatidylethanolamine conjugates (LC3-II). 130 nM C9-, 7.5 mM DCA- and C9+DCA-treated MCF-7- and

MCF-12A cells were stained with FITC-conjugated LC3-II antibodies and the fluorescence was measured via flow cytometry (previously described).

*Ultrastructure*

Transmission electron microscopy (TEM) was used to determine the ultrastructure of intracellular components. Exponentially growing cells were seeded and exposed to treatments (130 nM C9, 7.5 mM DCA and C9+DCA) for 24 h. Cells were fixed in glutaraldehyde (2.5%) in phosphate buffer (0.075M, pH 7.4-7.6) for 1 h. Thereafter, cells were fixed with aqueous osmium tetroxide for 30 min. Samples were dehydrated with increasing concentrations of ethanol and infiltrated with 30% quetol in ethanol for 1 h. Samples were polymerized at 60°C for at least 36 h before section. Ultra-thin sections were prepared with the aid of a microtome and were mounted on a copper grid. Samples were exposed to uranyl acetate (4%) before observed under the Multi-purpose Philips 301 Transmission Electron Microscope situated at Electron Microscopy Unit, University of Pretoria, Pretoria, RSA.

*Statistical considerations*

Each of the quantitative variables was statistically analysed for significance using the two-way analysis of variance (ANOVA) model with main factor treatment and cell type along with a term for the interaction between treatment and cell type. Sample sizes for quantitative experiments were at least three and data presented are representative of one (where applicable) of the three such experiments. The Student's *t*-test was applied where two groups of data were compared. Means are presented in bar charts, with T-bars referring to standard deviations. *P*-values of <0.05 were regarded as statistically significant. Qualitative experiments were repeated at least twice where data was obtained from of light- and electron microscopy.

## Results

*Cell viability*

The LDH assay measures the content of LDH released from cells due to damage to cell membranes as a result of necrosis and/or late apoptotic processes [43, 44]. LDH cell viability experiments demonstrated that cell viability in MCF-7- and MCF-12A cells decreased to 83.5% and 92.4% respectively compared to controls ($P < 0.05$) after 24 h treatment with C9+DCA (C9 = 130 nM and DCA = 7.5 mM) (Fig. 1). Neither C9- nor DCA-exposed cells showed significant cytosolic LDH enzymatic release after 24 h (Fig. 1). Our previous result demonstrated that 7.5 mM DCA sensitised 130 nM C9 towards the tumorigenic MCF-7 cells within 24 hours [9]. Thus, this test results confirmed that there are more viable MCF-12A cells than MCF-7 cells after 24 h treatment with C9+DCA ($P < 0.05$).

*Cell morphology via light microscopy*

Haematoxylin and eosin (H & E) staining was performed to observe cellular morphological changes in large scale. DCA (7.5 mM)-exposed MCF-7 and MCF-12A cells showed no morphological changes (Fig. 2B and 2F). C9 (130 nM)-exposed MCF-7 cells showed a marked decrease in cell density and an increase in cells arrested in metaphase (Fig. 2C). MCF-12A cells treated with C9 also showed an increase in the number of cells blocked in metaphase, however, the difference was not as big when compared to the C9-treated MCF-7 cells (Fig. 2G). After exposure to combination treatment of C9+DCA, MCF-7 cells exhibited a decrease in cell density (Fig. 2D) when compared to the vehicle-exposed tumorigenic cells. MCF-12A also showed decreases in cell density after exposure to combination treatment (Fig. 2H), however, this was less pronounced when compared to MCF-7-treated cells. Previous PlasDIC images also revealed the selective inhibition ability of C9+DCA towards MCF-7 cells [9].

MCF-7 and MCF-12A cells mitotic indices (Table 1) were derived from the H & E-stained slides by counting 1000 cells per slide [29]. Cells in the mitotic phase were subdivided into prophase, metaphase, anaphase, telophase and tripolar metaphase. Non-mitotic cells were subdivided into interphase and hypercondensed chromatin with the latter indicating the

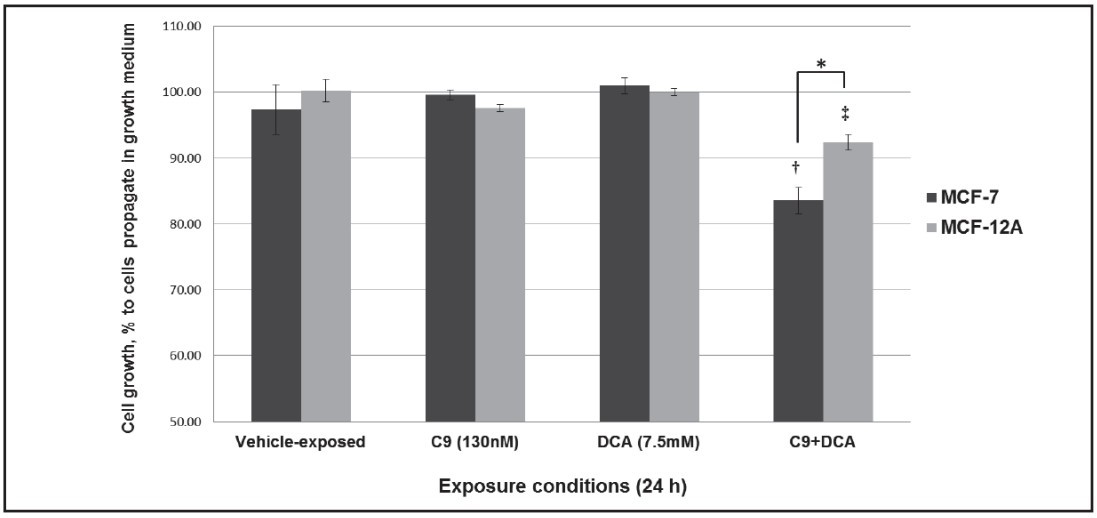


**Fig. 1.** LDH cell viability test of MCF-7 and MCF-12A cells. MCF-7 and MCF-12A cell growth expressed as a percentage of the control (cells propagated in medium with addition of vehicle, DMSO < 0.01%) after 24 h of exposure to 130 nM C9, 7.5 mM DCA and C9+DCA. †,‡, *P*-value < 0.05 after comparison of exposed cells and controls within the same cell line. *, *P*-value < 0.05 when MCF-7 and MCF-12A cells were compared for the same treatment.

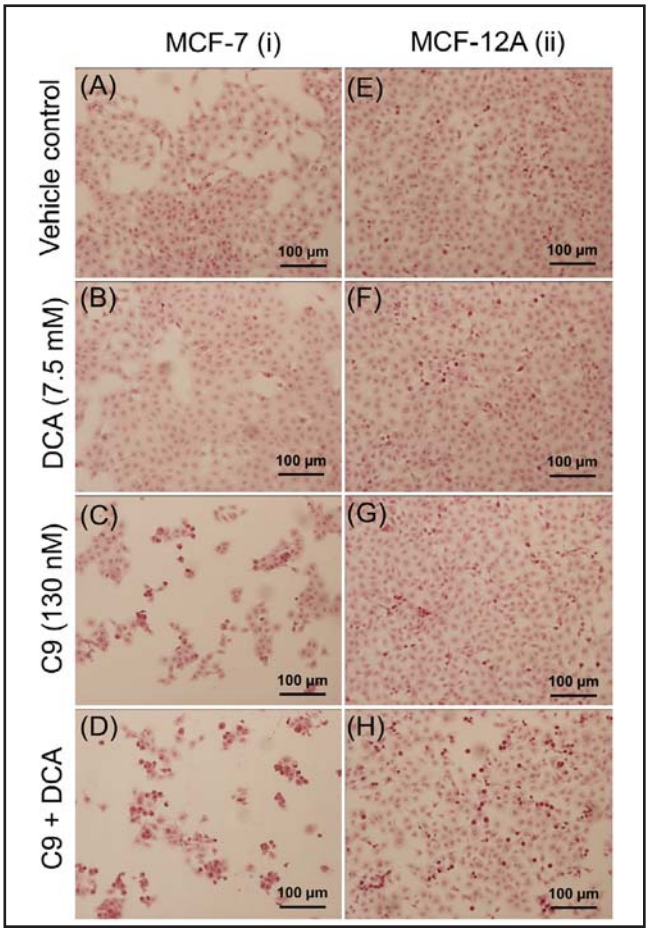


**Fig. 2.** Haematoxylin and eosin-stained images of MCF-7 and MCF-12A cells after 24 h treatment exposure. Haematoxylin and eosin-stained images of MCF-7 cells (i) (A-D) compared to MCF-12A cells (ii) (D-H) after 24 h exposure to different conditions. Vehicle-treated (A and E) cells were confluent and showed no sign of distress. Cells exposed to 7.5 mM of DCA (B and F) indicated no significant decrease in cell number. C9 (130 nM)-exposed MCF-7 cells (C) showed decreased cell density and an increase in metaphase. Cells exposed to C9 (130 nM) in combination of DCA (7.5 mM) (D and H) showed significant inhibition of cell growth and formation of apoptotic bodies.

number of cells undergoing apoptosis. DCA-exposed MCF-7 and MCF-12A cells showed no changes in mitotic indices. Treatment of MCF-7 cells with C9 and C9+DCA resulted in increased numbers of cells exhibiting metaphase morphology when compared to DMSO-exposed cells

**Table 1.** MCF-7 and MCF-12A cell mitotic indices. Data has been divided into vehicle-, C9-, DCA- or C9+DCA-exposed cells respectively. Cells in the mitotic phase were subdivided into prophase, metaphase, anaphase, telophase and tripolar metaphase. Non-mitotic cells were subdivided into interphase and hypercondensed chromatin, the latter indicating cells undergoing apoptosis

| MCF-7 | Vehicle control | C9 | DCA | C9+DCA |
|---|---|---|---|---|
| Mitotic cells | | | | |
| Prophase | 1.9 | 0.4 | 1.6 | 0.3 |
| Metaphase | 2.9 | 9.4 | 2.2 | 16.3 |
| Anaphase | 1.5 | 0.2 | 0.8 | 0 |
| Telophase | 1.2 | 0 | 0.9 | 0 |
| Tripolar metaphase | 0 | 0 | 0 | 0 |
| Non-mitotic cells | | | | |
| Interphase | 91.3 | 86.1 | 92.6 | 73.1 |
| Hypercondensed chromatin | 1.5 | 5.8 | 1.9 | 10.3 |
| MCF-12A | Vehicle control | C9 | DCA | C9+DCA |
| Mitotic cells | | | | |
| Prophase | 2.9 | 0.8 | 1.4 | 0.4 |
| Metaphase | 3.7 | 5.5 | 2.9 | 13.9 |
| Anaphase | 1.8 | 0.2 | 0.9 | 0 |
| Telophase | 2.4 | 0.1 | 1.8 | 0 |
| Tripolar metaphase | 0.7 | 1.9 | 1.0 | 0.8 |
| Non-mitotic cells | | | | |
| Interphase | 86.4 | 87.6 | 88.9 | 81.6 |
| Hypercondensed chromatin | 2.1 | 3.9 | 3.1 | 3.3 |

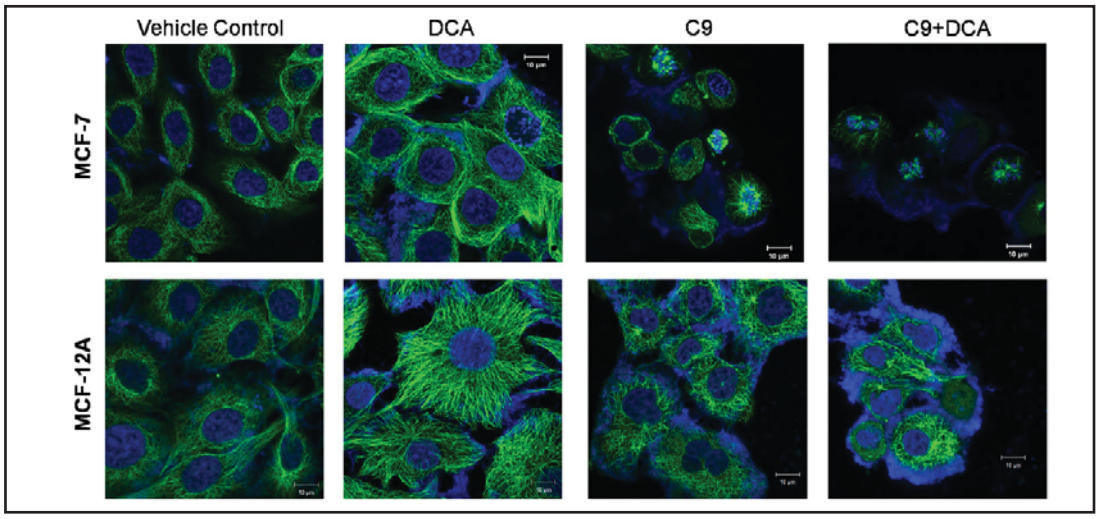


**Fig. 3.** Immunofluorescent staining of α-tubulin (green) for MCF-7 and MCF-12A cells. Fluorescent images of MCF-7 cells (top row) compared to MCF-12A cells (bottom row) after 24h of exposure to DCA (7.5 mM), C9 (130 nM) and C9+DCA. Vehicle-treated MCF-7 and MCF-12A cells were confluent and showed no sign of distress. DCA-exposed cells showed no significant decrease in cell number, but displayed slightly larger and flattened morphology. C9 (130 nM)-exposed MCF-7 and MCF-12A cells decreased in cell number; MCF-7 displayed formation of abnormal spindle, as well as cell arrested in metaphase after treatment. Cells exposed to C9 (130 nM) in combination of DCA (7.5 mM) showed significant inhibition of cell growth, abnormal spindle formation and fragmentation of genomic material.

(Table 1: DMSO - 2.9%, C9 - 9.4% C9+DCA - 16.3%). These treatments (C9 and C9+DCA) also increased the count for cells exhibiting hypercondensed chromatin when compared to DMSO-exposed cells (Table 1: DMSO - 1.5%, C9 - 5.8%, C9+DCA - 10.3%). This result shows that compound C9 has antimitotic effects and also promotes apoptosis. Furthermore, the addition of DCA with C9 exhibited additive effects, where the number of cells in metaphase and cells exhibiting hypercondensed chromatin almost doubled compared to C9-exposed MCF-7 cells (Table 1).

*Confocal microscopy*

Confocal microscopy revealed the cytoskeletal microtubule architecture of α-tubulin for both MCF-7 and MCF-12A cells. An increase in cell size of both MCF-7 and MCF-12A cells

**Table 2.** Differentially expressed genes mapped to functional cellular pathways in MCF-7 and MCF-12A cells exposed to 130 nM of C9 and 7.5 mM of DCA for 24 h. M-values represent a log2-fold change between two or more experimental conditions

| GeneBank number | Gene name | Description | MCF-7 | MCF-12A |
|---|---|---|---|---|
| | | | Log M | |
| Cell proliferation and cell senescence | | | | |
| NM_014417 | BBC3 | BCL2 binding component 3 | 1.217 | 0.904 |
| NM_006879 | MDM2 | Mdm2, transformed 3T3 cell double minute 2, p53 binding | 1.111 | 0.624 |
| NM_001731 | BTG1 | B-cell translocation gene 1, anti-proliferative | 0.740 | 0.798 |
| NM_005766 | FARP1 | FERM, RhoGEF (ARHGEF) and pleckstrin domain protein 1 | 0.200 | 0.513 |
| NM_005657 | TP53BP1 | Tumor protein p53 binding protein, 1 | 0.191 | |
| NM_178234 | TUSC3 | Tumor suppressor candidate 3 | 0.172 | |
| NM_004083 | DDIT3 | DNA-damage-inducible transcript 3 | | 1.551 |
| NM_005118 | TNFSF15 | Tumor necrosis factor (ligand) superfamily, member 15 | | 0.775 |
| NM_015124 | DIP | Death-inducing-protein (DIP) | | 0.694 |
| NM_003932 | ST13 | Suppression of tumorigenicity 13 (Hsp70 interacting protein) | -0.254 | |
| NM_006451 | PAIP1 | Poly(A) binding protein interaction protein 1 | -0.543 | |
| NM_002467 | MYC | v-myc Myelocytomatosis viral oncogene homolog | | -0.707 |
| NM_006761 | YWHAE | Tyrosine 3-monooxygenase/tryptophan 5-monooxygenase activation protein | -0.179 | -0.585 |
| NM_006509 | RELB | v-rel Reticuloendotheliosis viral oncogene homolog B, nuclear factor of kappa light polypeptide gene enhancer in B-cells 3 | 0.266 | 0.885 |
| NM_002228 | JUN | Jun oncogene | 0.155 | |
| NM_201612 | IKIP | IKK interacting protein | 0.440 | 0.521 |
| Cell cycle, cytoskeleton and DNA repair | | | | |
| NM_001614 | ACTG1 | Actin, gamma 1 | -0.454 | -0.610 |
| NM_005524 | HES1 | Hairy and enhancer of split 1 | -0.291 | -2.020 |
| NM_005517 | HMGN2 | High-mobility group nucleosomal binding domain 2 | -0.430 | -0.545 |
| NM_006306 | SMC1A | Structural maintenance of chromosomes 1A | -0.287 | -0.604 |
| NM_032704 | TUBA6 | Tubulin, alpha 6 | -0.366 | -0.653 |
| NM_006000 | TUBA1 | Tubulin, alpha 1 | -0.482 | |
| NM_018943 | TUBA8 | Tubulin, alpha 8 | -0.425 | |
| NM_001069 | TUBB2A | Tubulin, beta 2A | -0.282 | |
| NM_002374 | MAP2 | Microtubule-associated protein 2 | | 0.574 |
| NM_003980 | MAP7 | Microtubule-associated protein 7 | -0.689 | |
| NM_001618 | PARP1 | Poly (ADP-ribose) polymerase family, member 1 | -0.195 | |
| NM_005484 | PARP2 | Poly (ADP-ribose) polymerase family, member 2 | | 0.492 |
| NM_024615 | PARP8 | Poly (ADP-ribose) polymerase family, member 8 | | 0.929 |
| NM_001924 | GADD45A | Growth arrest and DNA-damage-inducible, alpha | | 0.793 |
| NM_001237 | CCNA2 | Cyclin A2 | | -0.373 |
| NM_053056 | CCND1 | Cyclin D1 | | -0.729 |
| NM_000321 | RB1 | Retinoblastoma 1 | | -0.544 |
| NM_002577 | PAK2 | p21 (CDKN1A)-activated kinase 2 | | -0.900 |
| NM_003390 | WEE1 | WEE1 homolog | 0.257 | |
| NM_003858 | CCNK | Cyclin K | -0.479 | |
| NM_007295 | BRCA1 | Breast cancer 1, early onset | -0.209 | |
| NM_015894 | STMN3 | Stathmin-like 3 (STMN3) | -0.289 | |
| Metabolism | | | | |
| NM_000927 | ABCB1 | ATP-binding cassette, sub-family B (MDR/TAP), member 1 | | 0.679 |
| NM_005688 | ABCC5 | ATP-binding cassette, sub-family C (CFTR/MRP), member 5 | | 0.534 |
| NM_006066 | AKR1A1 | Aldo-keto reductase family 1, member A1 (aldehyde reductase) | 0.439 | |
| NM_005603 | ATP8B1 | ATPase, Class I, type 8B, member 1 | 0.460 | |
| NM_201444 | DGKA | Ddiacylglycerol kinase, alpha 80kDa | 0.383 | |
| NM_002633 | PGM1 | Phosphoglucomutase 1 | 0.334 | |
| NM_181523 | PIK3R1 | Phosphoinositide-3-kinase, regulatory subunit 1 (p85 alpha) | -0.181 | |

continued

was observed after 24 h of exposure to DCA (7.5 mM) when compared to the control (Fig. 3, DCA). An increased portion of MCF-7 cells showed characteristics of cells arrested in metaphase and abnormal spindle formation after exposure to C9 (130 nM) for 24 h (Fig. 3, C9). The combination-exposed tumorigenic cells exhibited characteristics that were similar to C9-exposed MCF-7 cells with additional hallmarks of fragmented DNA and destruction of α-tubulin architecture (Fig. 3, C9+DCA). Furthermore, abnormal multinucleated MCF-12A cells after treatment with C9 for 24 h was demonstrated (Fig. 3, C9). The effect of the

| GeneBank number | Gene name | Description | MCF-7 Log M | MCF-12A |
|---|---|---|---|---|
| Reactive oxygen species metabolism | | | | |
| NM_002032 | FTH1 | ferritin, heavy polypeptide 1 | 0.201 | 0.604 |
| NM_000146 | FTL | Ferritin, light polypeptide | 0.272 | |
| NM_006701 | TXNL4A | Thioredoxin-like 4A | -0.320 | |
| NM_017853 | TXNL4B | Thioredoxin-like 4B | -0.241 | |
| NM_006793 | PRDX3 | Peroxiredoxin 3 (PRDX3), nuclear gene encoding mitochondrial protein | -0.176 | |
| NM_004110 | FDXR | Ferredoxin reductase, nuclear gene encoding mitochondrial protein | | 0.741 |
| NM_031894 | FTHL17 | Ferritin, heavy polypeptide-like 17 | | 0.567 |
| NM_000846 | GSTA2 | Glutathione S-transferase A2 | | 1.133 |
| NM_000625 | NOS2A | Nitric oxide synthase 2A (inducible, hepatocytes) | | 0.840 |
| NM_000603 | NOS3 | Nitric oxide synthase 3 (endothelial cell) | | 0.419 |
| NM_002970 | SAT1 | Spermidine/spermine N1-acetyltransferase 1 | | 1.402 |
| NM_175839 | SMOX | Spermine oxidase | | 1.007 |
| NM_000454 | SOD1 | Superoxide dismutase 1 | | 0.614 |
| NM_001024465 | SOD2 | Superoxide dismutase 2, mitochondrial | | 1.159 |
| NM_002133 | HMOX1 | heme oxygenase (decycling) 1 (HMOX1), mRNA | | -0.429 |
| NM_006819 | STIP1 | Stress-induced-phosphoprotein 1 (Hsp70/Hsp90-organizing protein) | | -0.729 |
| Regulation of transcription | | | | |
| NM_133467 | CITED4 | Cbp/p300-interacting transactivator | 0.343 | 0.728 |
| NM_006079 | CITED2 | Cbp/p300-interacting transactivator, with Glu/Asp-rich carboxy-terminal domain, 2 | | -0.901 |
| NM_012138 | AATF | Apoptosis antagonizing transcription factor | | -0.666 |
| NM_001950 | E2F4 | E2F transcription factor 4, p107/p130-binding | | -0.887 |
| NM_001968 | EIF4E | Eukaryotic translation initiation factor 4E | -0.501 | -1.799 |
| NM_005194 | CEBPB | CCAAT/enhancer binding protein, beta | 0.284 | |
| NM_001455 | FOXO3A | Forkhead box O3A (FOXO3A) | 0.131 | |
| NM_005801 | EIF1 | Eukaryotic translation initiation factor 1 | -0.389 | |
| NM_001968 | EIF4E | Eukaryotic translation initiation factor 4E | -0.501 | |
| NM_005252 | FOS | v-fos FBJ murine osteosarcoma viral oncogene homolog | 0.557 | |
| NM_000937 | POLR2A | Polymerase (RNA) II (DNA directed) polypeptide A | -0.161 | |
| ENST00000373575 | ENST00000373575 | Eukaryotic translation initiation factor 4E type 2 | -0.193 | |
| Protein kinases and phosphatases | | | | |
| NM_001007271 | DUSP13 | Dual specificity phosphatase 13 | 0.483 | 0.488 |
| NM_017572 | MKNK2 | MAP kinase interacting serine/threonine kinase 2 | 0.421 | 0.706 |
| NM_002831 | PTPN6 | Protein tyrosine phosphatase, non-receptor type 6 | 0.156 | |
| NM_000455 | STK11 | Serine/threonine kinase 11 | 0.323 | |
| NM_203351 | MAP3K3 | Mitogen-activated protein kinase kinase kinase 3 | 0.116 | -0.610 |
| NM_145109 | MAP2K3 | Mitogen-activated protein kinase kinase 3 (MAP2K3) | | -1.453 |
| NM_138957 | MAPK1 | Mitogen-activated protein kinase 1 | | -0.462 |
| NM_002752 | MAPK9 | Mitogen-activated protein kinase 9 | 0.145 | |
| NM_001315 | MAPK14 | Mitogen-activated protein kinase 14 | -0.253 | |

combination treatment on MCF-12A cells is moderate in comparison with MCF-7 cells that were treated under the same exposure conditions (Fig. 3, C9+DCA).

*Microarray gene expression analysis*

Global gene expression analysis was conducted by employing the Agilent's Human 1A oligonucleotide microarray slides. After treatment of C9+DCA (24 h), 684 and 830 genes were considered statistically significantly differentially ($P < 0.05$) expressed in MCF-7 and MCF-12A cells respectively. Differentially expressed genes exclusively responsive to C9+DCA-treated (24 h) MCF-7 and MCF-12A cells were mapped and summarized in Table 2 to cell death, cell cycle, cytoskeleton, metabolism, transcription, epigenetic regulation, protein kinases and phosphatases, reactive oxygen species metabolism and ribosomal proteins.

As shown in Table 2, C9+DCA induced the expression of a number of genes related to the p53 pathway in MCF-7 cells including tumour protein p53 binding protein 1 (*TP53BP1*), transformed 3T3 cell double minute 2 (*MDM2*) and BCL2 binding component 3 (*BBC3/PUMA*). Few apoptotic-related genes were commonly up regulated in both cell lines after 24 h treatment such as *BBC3/PUMA*, *MDM2*, Cbp/p300-interacting transactivator (*CITED4*), B-cell translocation gene 1 (*BTG1*), inhibitor of NF-κB (IκB) kinase (IKK) interacting protein

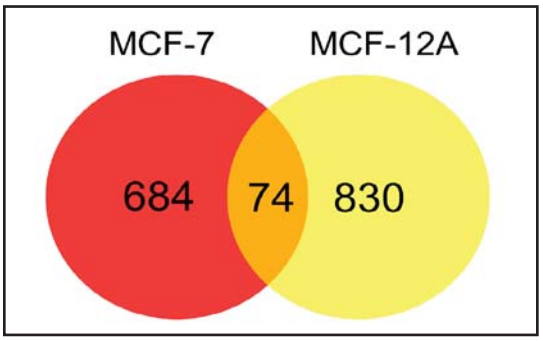


**Fig. 4.** GeneVenn diagram showing 74 commonly affected genes in MCF-7 and MCF-12A cells after 24 h exposure to C9 (130 nM) in combination with DCA (7.5 mM). Treatment C9+DCA caused 610 and 756 statistically differentially expressed genes in MCF-7 and MCF-12A cell lines respectively.

(IKIP), dual-specificity phosphatase 13 (*DUSP13*) and ferritin, heavy polypeptide 1 (*FTH1*).

Cell growth and proliferation depend on the general mRNA translation processes. The circularization of the mRNA 5' cap and 3' poly(A) tail structure is dependent on the interactions between eukaryotic initiation factor 4G (eIF4G) and poly(A) binding protein (PABP) [45]. Poly(A) binding protein interaction protein 1 (PAIP1) is able to interact with both eIF4G [46] and PABP to stimulate translation [45]. In this study, the expression of *PAIP1* was down regulated in MCF-7 cells after C9+DCA-treatment for 24 h. Moreover, two genes involved in DNA repair namely poly (ADP-ribose) polymerases 1 (*PARP1*) and breast cancer 1 (*BRCA1*) were down regulated in MCF-7 cells. The combination treatment also affected several genes of the PI3K/AKT/mTOR pathway: eukaryotic translation initiation factor 1 (*EIF1*); eukaryotic translation initiation factor 4E (*EIF4E*); mitogen-activated protein kinase 14 (*MAPK14*), phosphoinositide-3-kinase regulatory subunit 1 (*PIK3R1*); protein tyrosine phosphatase non-receptor type 6 (*PTPN6*); tyrosine 3-monooxygenase/tryptophan 5-monooxygenase activation protein (*YWHAE*); proto-oncogene *c*-Fos (*FOS*) and jun proto-oncogene (*JUN*) in MCF-7 cells.

The NF-κB pathway is important for normal mammary gland development, as well as breast cancer formation [47]. *v*-rel Reticuloendotheliosis viral oncogene homolog B, nuclear factor of kappa light polypeptide gene enhancer in B-cells 3 (*RELB*) and IKIP genes were up regulated in both cell lines. The Notch pathway target gene hairy and enhancer of split 1 (*HES1*) represses the expression of a cell-cycle inhibitor cyclin-dependent kinase inhibitor, $p27^{Kip1}$, independently of a cell differentiation role [48]. *HES1* expression was down regulated in both cell lines after treatment of C9+DCA, thus indicating the possible activation of $p27^{Kip1}$ and cell cycle inhibition. Cyclin K encoding gene *CCNK* expression was down regulated in MCF-7 cells treated with C9+DCA. Cyclin K plays an important role in transcriptional-elongation regulation by its interaction with RNA polymerase II C-terminal domain [49].

A number of genes that are involved in reactive oxygen species metabolism were down regulated in MCF-7 treated cells such as thioredoxin-like 4A (*TXNL4A*), thioredoxin-like 4B (*TXNL4B*) and peroxiredoxin 3 (*PRDX3*). Ferritin, both heavy and light polypeptide genes (*FTH1* and *FTL*) were induced in MCF-7 cells. Free iron is a potent oxidant that damages the cell through reaction with hydrogen peroxide with formation of hydroxyl radical. In normal cells, lysosomes utilize the iron-binding proteins such as apoferritin, ferritin, metallothioneins and heat shock protein of 70 kDa (HSP70) to reduce tension exerted by free Fe (II) before protein degradation process occurs [50, 51].

The treatment of C9+DCA, especially with C9 being the antimitotic agent, suppressed a large number of genes related to cellular structural integrity in both cell lines. Actin (*ACTG1*), microtubule-associated protein 7 (*MAP7*), tubulin alpha 1, 6 and 8, as well as tubulin beta 2A (*TUBA1*, *TUBA6*, *TUBA8* and *TUBB2A*) genes were down regulated in both cell lines. These structure-related genes encode proteins that are important to cell motility and maintenance of the cytoskeleton [52-54].

For C9+DCA-exposed MCF-12A cells, a number of genes related to p53 pathway were differentially expressed. Similarly to the MCF-7 gene expression profile *BBC3/PUMA*, *MDM2* were up regulated. Conversely, proto-oncogene *c*-Myc (*MYC*), cyclin D1 (*CCND1*) and

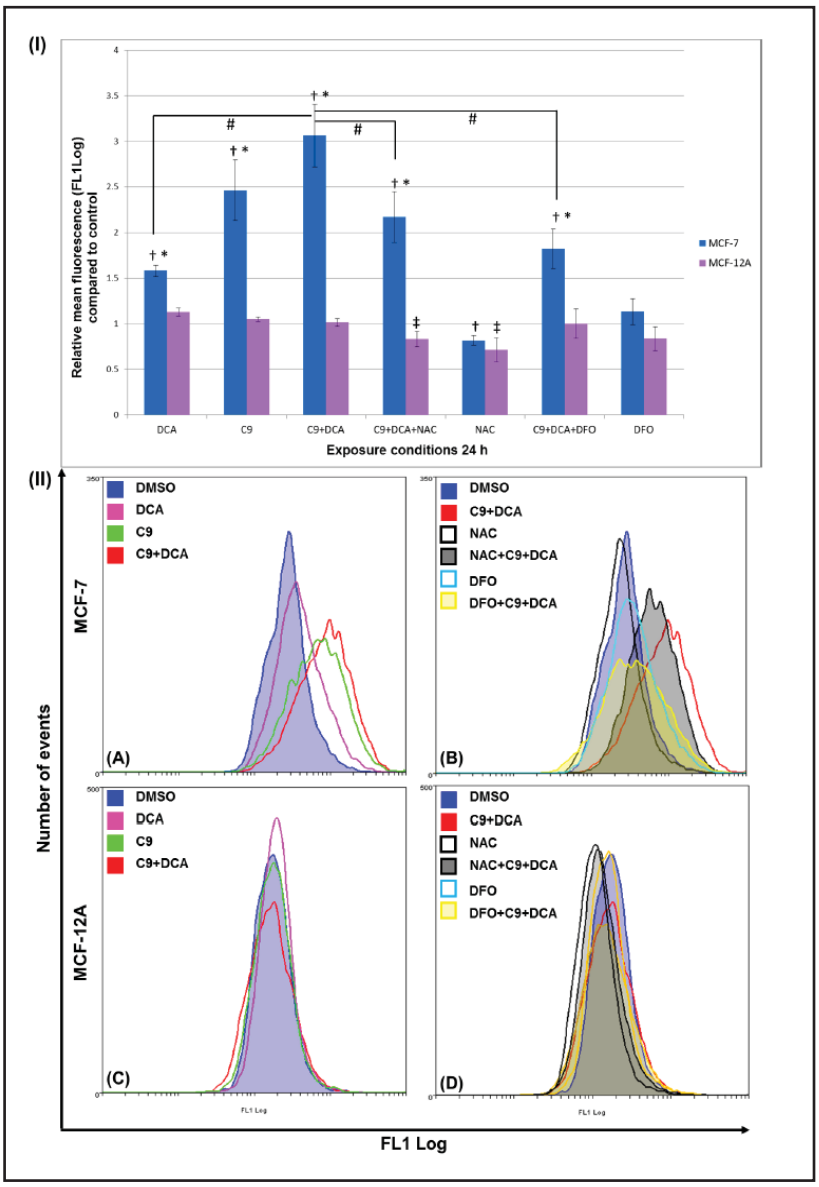


**Fig. 5.** Oxidative stress test by means of $H_2O_2$/$Fe^{2+}$ measurement via DCF fluorescence. Relative mean fluorescence (FL1 Log) of C9-, DCA-, and C9+DCA-treated MCF-7 and MCF-12A cells compared to vehicle-exposed controls (i). Flow cytometric data of FL1 Log versus count illustrated the x-mean shift (ii). The influence of the antioxidant, NAC (5 mM), and a ferric iron chelator, desferoxamin (100 µM), were investigated and results showed NAC and DFO reduced effect of C9+DCA treatment on MCF-7 cells. †, ‡*P*-value < 0.05 after comparison of exposed cells and controls within the same cell line. **P*-value < 0.05 when MCF-7 and MCF-12A cells were compared for the same treatment. #*P*-value < 0.05 when C9+DCA-treatment were compared with other treatments within MCF-7 cell line.

retinoblastoma 1 (*RB1*) were down regulated in MCF-12 A cells. DNA-damage-inducible transcript 3 (DDIT3) and growth arrest and DNA-damage-inducible (GADD45A) genes expression were induced in MCF-12A cells.

ATP-binding cassette, sub-family B (MDR/TAP), member 1 (*ABCB1*) and ATP-binding cassette, sub-family C (CFTR/MRP) and member 5 (*ABCC5*) multidrug-resistant genes were induced in treated MCF-12A cells, which perhaps partly accounted for the resistance to treatment. *ABCB1* functions as an energy-dependent drug efflux transporter that lowers concentrations of various anticancer drugs, such as colchicine, paclitaxel, doxorubicin and vinblastine [55, 56].

Genes involved in ROS metabolism; namely, *FTH1*, glutathione S-transferase A2 (*GSTA2*); nitric oxide synthase 2A (*NOS2A*); spermine oxidase (*SMOX*); superoxide dismutase 1 (*SOD1*) and superoxide dismutase 2 mitochondrial (*SOD2*) were up regulated. The ferredoxin reductase gene is reported to regulate the p53 family and as a result sensitises cells to oxidative stress-induced apoptosis [57]. The ferredoxin reductase (*FDXR*) gene was down regulated. FDXR gene product ferredoxin reductase protein transfers electrons from NADPH to cytochrome P450 via ferredoxin in mitochondria [58].

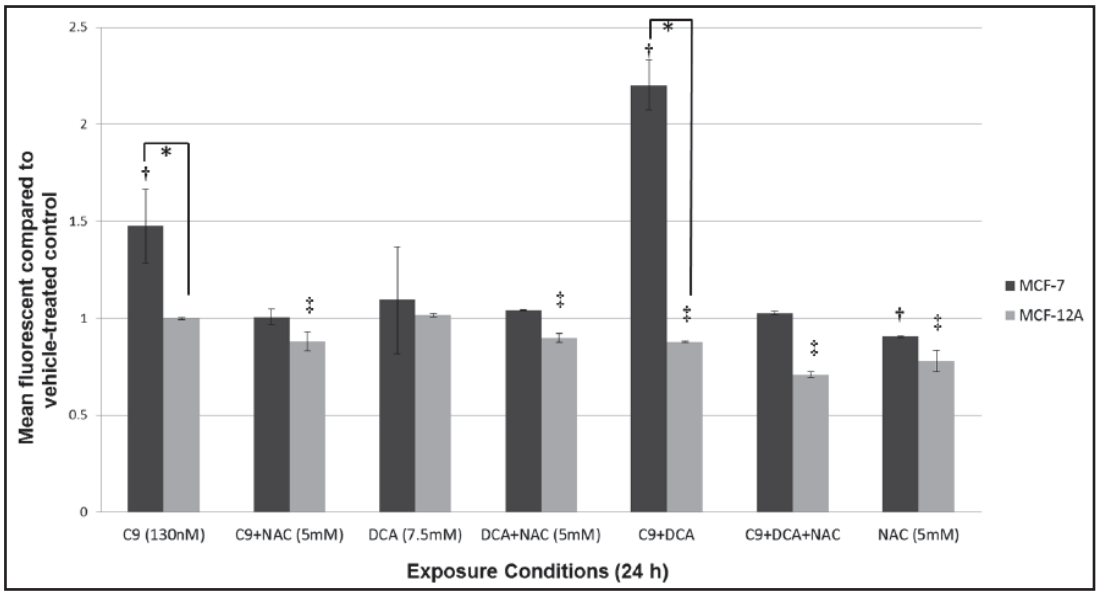


**Fig. 6.** MitoCapture™ cationic dye detection of mitochondrial membrane potential (ΔΨm) depolarization. Treatment with C9 (130 nM) and C9+DCA increased MCF-7 cell mitochondrial membrane potential (ΔΨm) depolarization compared to vehicle-exposed controls to 1.5- and 2.2-fold respectively ($P < 0.05$). None of the treatments influenced ΔΨm depolarization of MCF-12A cells. The influence of the antioxidant, NAC (5 mM), was investigated and used in conjunction with C9 (130 nM), DCA (7.5 mM) and C9+DCA. NAC attenuated the ΔΨm depolarization induced by C9 (1.5-fold) and C9+DCA (2.2-fold) on MCF-7 cells to 1.0 ($P < 0.05$). †*P*-value < 0.05 after comparison of exposed cells and controls within the same cell line. **P*-value < 0.05 when MCF-7 and MCF-12A cells were compared for the same treatment.

*Oxidative stress test*

Gene-expression analyses suggested that oxidative stress may play an important role in cell signalling in C9+DCA-treated tumorigenic MCF-7 and non-tumorigenic MCF-12A cells. In order to explore and determine the hypothesis of abrogated oxidative stress of C9+DCA-treated cells, flow cytometric analyses of MCF-7 cells loaded with the $H_2O_2/Fe^{2+}$-sensitive fluorophore $H_2$DCF-DA were utilized. This result showed DCA-, C9-, and C9+DCA-treated MCF-7 cells (24 h) had a statistically significant increase in DCF fluorescence signal compared to vehicle-exposed control ($P < 0.05$) (Fig. 5I and 5IIA). None of the treatment, neither the combination nor alone, caused the increased level of $H_2O_2/Fe^{2+}$ for MCF-12A cells (Fig. 5I and 5IIC). DCA-exposed MCF-7 cells showed 1.5 fold increases in $H_2O_2/Fe^{2+}$ fluorescence signal level but not in MCF-12A cells (Fig. 5I). These result imply DCA has the ability to induce ROS production in tumorigenic cells. A possible explanation is DCA inhibited the activity of PDK and forced the MCF-7 cell to use the mitochondria for energy production. As a result, OXPHOS was stimulated and production of ROS increased. In addition, C9- and C9+DCA-treated MCF-7 cells (24 h) had a significant increase in DCF fluorescence signal compared to DCA-treated samples ($P < 0.05$). The addition of NAC (ROS inhibitor) and DFO (iron chelator) attenuated the effect of C9+DCA on MCF-7 cells ($P < 0.05$) (Fig. 5I and 5IIB). This data suggest that treatment C9 probably increased the cytosolic labile iron pool through its antimitotic ability, DCA sensitised C9 towards the tumorigenic cells by the Fenton-type of reaction. The Fenton reaction is when ferrous ions ($Fe^{2+}$) react with hydrogen peroxide to form the highly reactive hydroxyperoxyl radicals ($H_2O_2 + Fe^{2+} \rightarrow Fe^{3+} + {}^{\bullet}OH + OH^-$) [59].

*Mitochondrial membrane potential (ΔΨm) assay*

A 1.5- and 2.2-fold ΔΨm increase in depolarisation in MCF-7 cells compared with controls ($P < 0.05$), but not in MCF-12A cells were observed after treatment with C9 and C9+DCA for 24 h, respectively (Fig. 6). Treatment of only DCA did not cause any membrane

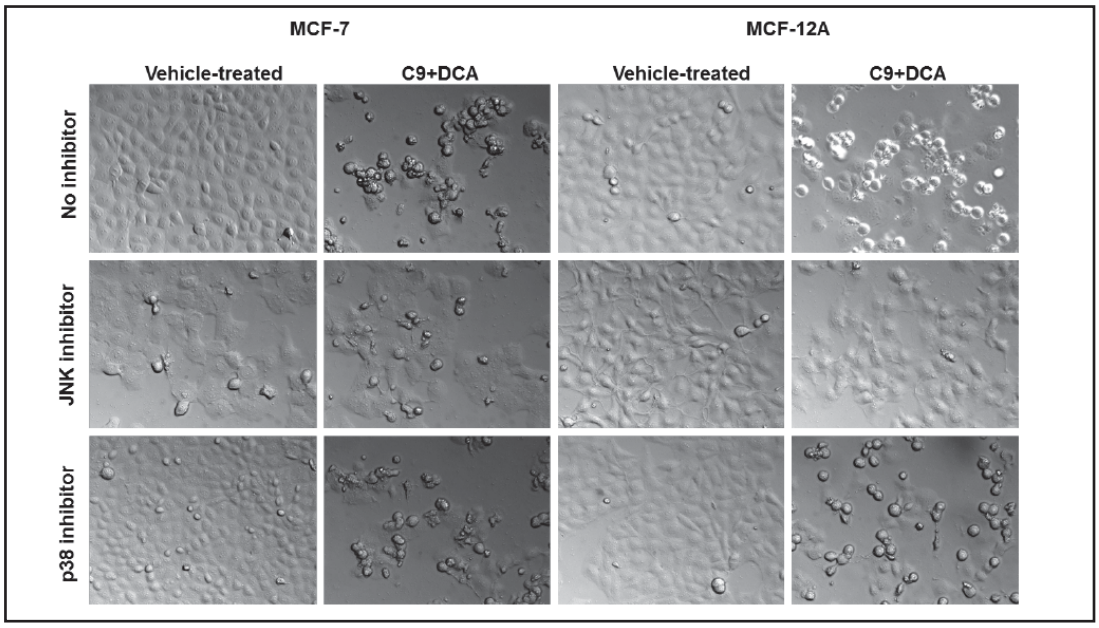


**Fig. 7.** Optical transmitted light differential interference contrast images of MCF-7 cells and MCF-12A after 24 h exposure to different conditions. Vehicle-treated cells were confluent and showed no sign of distress. Cells exposed to C9 (130 nM) in combination with DCA (7.5 mM) showed significant inhibition of cell growth. JNK inhibitor SP600125-exposed (20 μM) untreated MCF-7 and MCF-12A cells were negatively affected with decreased density; however, it reduced the effect of C9+DCA on these cells. The addition of a p38 inhibitor, SB 239063 (15 μM), did not change MCF-7 and MCF-12A cells from its original appearance. (Magnification 20 X).

potential loss in either MCF-7 or MCF-12A cells (Fig. 6). In order to establish the possible link between ROS and ΔΨm depolarisation, NAC (5 mM) was utilized as a broad spectrum ROS inhibitor. Addition of NCA to untreated cells reduced the mitochondrial membrane potential in both cell lines (Fig. 6). Furthermore, NAC completely attenuated the anti-mitotic compound C9 and the combination of C9+DCA's effects on MCF-7 cells ($P < 0.05$) (Fig. 6). This data suggests that oxidative signalling has a causal role in the induction of mitochondrial membrane depolarization in MCF-7 cells.

*MAP kinase inhibition study*

The observation that ROS plays a role in inducing mitochondrial membrane potential suggests that stress-activated protein kinases such as JNK and p38 may play role in the signalling of C9+DCA. These kinases are known to be able to phosphorylate JNK and p38. Therefore, a JNK inhibitor (JNKi) SP600125 (20 μM) and p38α inhibitor (p38i) SB239063 (15 μM) were included in the experiments to test whether these pathways play roles with regard to activation/deactivation of Bcl-2 protein in MCF-7 and MCF-12A cells. NAC had a protective effect on the MCF-7 cells when added together with C9+DCA in these cells.

The addition of JNK inhibitor to MCF-7 and MCF-12A cells decreased cell density compared to the control, this was not observed when p38α inhibitor was added (Fig. 7). In fact, the addition of JNK inhibitor to MCF-7 and MCF-12A cells treated with C9+DCA prevented cell death to some extent compared to C9+DCA-treated controls and this was not observed when p38α inhibitor was added (Fig. 7).

*Bcl-2 expression and phosphorylation status*

The DCF test and the ΔΨm depolarisation results suggest that the C9+DCA-treated MCF-7 cell might utilize the intrinsic pathway to induce apoptosis. Bcl-2 is an anti-apoptotic protein that plays a role in modulating the membrane potential of mitochondria. An

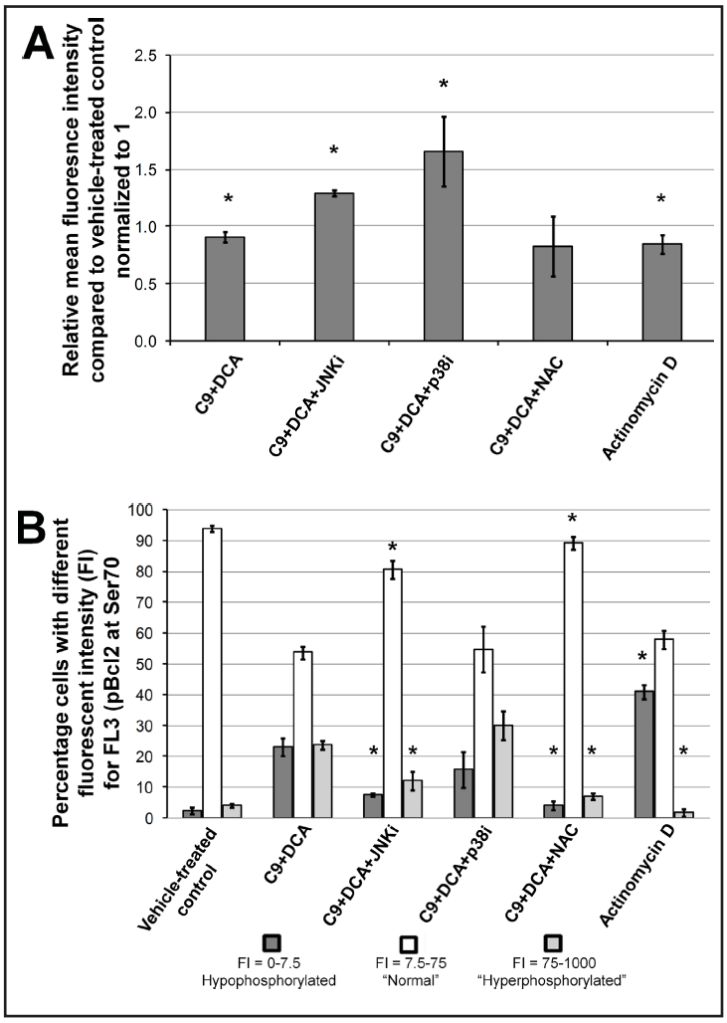


**Fig. 8.** MCF-7 cells total Bcl-2 protein expression (A) and phosphorylation statuses (B) after 24 h exposure. Exposure conditions: C9 (130 nM)+DCA (7.5 mM), C9+DCA+p38i (SB239063: 15 μM), C9+DCA+JNKi (SP600125: 20 μM) and actinomycin D (2 μg/ml). Total Bcl-2 expression was significant lowered in C9+DCA- and actinomycin D-treated MCF-7 cells compared to DMSO control (*, $P < 0.05$) (A). Bcl-2 levels increased in C9+DCA+p38i- and C9+DCA+JNKi-exposed MCF-7 cells (*, $P < 0.05$) (A). C9+DCA treatment resulted in a decrease in the number of cells with an FL3 FI of 7.5-75 (normal) when compared to the vehicle-exposed control (B). Both JNK inhibition and NAC treatment in C9+DCA-treated cells also decreased the number of cells with an FL3 FI of 7.5-75 (normal) when compared to the vehicle-treated control. However, this decrease was statistically significantly less when compared to the C9+DCA-treated cells (*, $P < 0.05$) (B).

intracellular increase in the expression of Bcl-2 protein is associated with its anti-apoptotic effects by preventing mitochondrial depolarization through its interaction with and ultimate inhibition of Bax (a pro-apoptotic protein) [38]. The phosphorylation status of Bcl-2 also determines whether it is pro- or anti-apoptotic. The observations that C9+DCA induces the expression of BBC3/PUMA and causes mitochondrial membrane depolarization suggest that Bcl-2 may play a mechanistic role in the effects of C9+DCA.

The total expression of Bcl-2 in the treated MCF-7 samples was statistically significantly lower in C9+DCA-treated cells compared to vehicle-exposed controls (Fig. 8A). Decreased expression of total Bcl-2 in C9+DCA-treated cells suggests that the anti-apoptotic effects of Bcl-2 may be inhibited by C9+DCA treatment. Total Bcl-2 expression increased in C9+DCA+p38i- and C9+DCA+JNKi-exposed MCF-7 cells (Fig. 8A). This result suggested that p38 and JNK pathways might act as important pro-apoptotic factors in treated MCF-7 cells. In MCF-12A cells, total Bcl-2 expression was unaffected in cells exposed to C9+DCA (Fig. 9A). The total Bcl-2 expression increased in C9+DCA+JNKi-exposed MCF-12A cells (Fig. 9A). This result demonstrated the combination treatment has ability of altering the total Bcl-2 expression in tumorigenic cells, but not in non-tumorigenic cells. The JNK pathway is an important signalling pathway to both MCF-7 and MCF-12A cells.

When measuring the phosphorylation status (FL3 = pBcl-2 at $Ser^{70}$) of MCF-7 and MCF-12A cells, it was observed that > 90% of vehicle-exposed cells had a fluorescence intensity (FI) of 7.5-75 (Fig. 8B and Fig. 9B). In MCF-7 cells, C9+DCA treatment resulted in a decrease in Bcl-2 normal phosphorylation status and, in turn, increased in hypo- and hyper-phosphorylation status of Bcl-2 $Ser^{70}$ (Fig. 8B). The anti-proliferative effect of C9+DCA

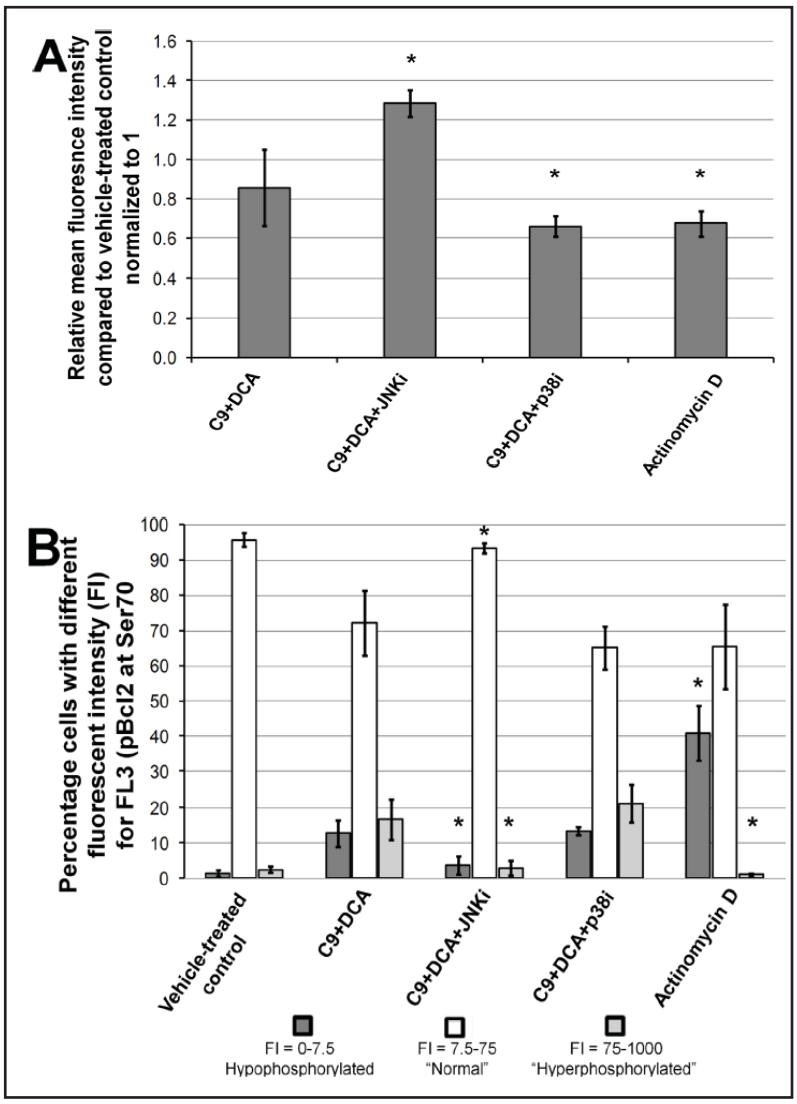


**Fig. 9.** MCF-12A cells total Bcl-2 protein expression (A) and phosphorylation statuses (B) after 24 h exposure. Exposure conditions: C9 (130 nM)+DCA (7.5 mM), C9+DCA+p38i (SB239063: 15 μM), C9+DCA+JNKi (SP600125: 20 μM) and actinomycin D (2 μg/ml). Total Bcl-2 expression was unaffected in MCF-12A cells exposed to C9+DCA (A). However, it was significant lowered in C9+DCA+p38i- and actinomycin D-treated cells compared to DMSO control (*, $P < 0.05$) (A). C9+DCA treatment resulted in a decrease in the number of cells with an FL3 FI of 7.5-75 (normal) when compared to the vehicle-exposed control (B). JNK inhibition in C9+DCA-treated cells did not exhibit significant differences when compared to the vehicle-exposed control. This decrease was statistically significantly less when compared to the C9+DCA-treated cells (*, $P < 0.05$) (B).

treatment on MCF-7 cells was affected when JNK inhibitor and ROS inhibitor (NAC) were added ($P < 0.05$). This result showed the ROS and JNK activation in C9+DCA-treated cells has pro-apoptotic effects on Bcl-2. Similar results were observed in the MCF-12A cell line (Fig. 9B). However, the effect was more pronounced in the MCF-7 cell line when compared to the MCF-12A cell line (Fig. 9B).

Hypo-phosphorylation of Bcl-2 at serine 70 is pro-apoptotic [38]. Hyper-phosphorylation of Bcl-2 at $Ser^{70}$ single-sited is anti-apoptotic, while multi-site hyper-phosphorylation at $Ser^{70}$, $Trp^{69}$ and $Ser^{87}$ is pro-apoptotic [40]. It is also known that multi-site phosphorylation of Bcl-2 is associated with a $G_2$/M block in MCF-7 and MDA-MB-231 cells [40]. C9 is an antimitotic compound and blocks cells in $G_2$/M. Our data showed increased hypo- and hyper-phosphorylation status of Bcl-2 at serine 70 after treatment of C9+DCA, suggesting that the combination treatment can result in multi-site phosphorylation of Bcl-2.

*Caspase 7 activity*

Caspase 7 is an executioner caspase that plays a key role in apoptosis. Primary antibodies against active caspase 7 were used to study protein expression changes in the MCF-7 and MCF-12A cells after 24 h treatment of C9-, DCA- and C9+DCA. Actinomycin D (0.2 μg/ml) was used as a positive control for apoptosis induction and to ensure the correct protocol was

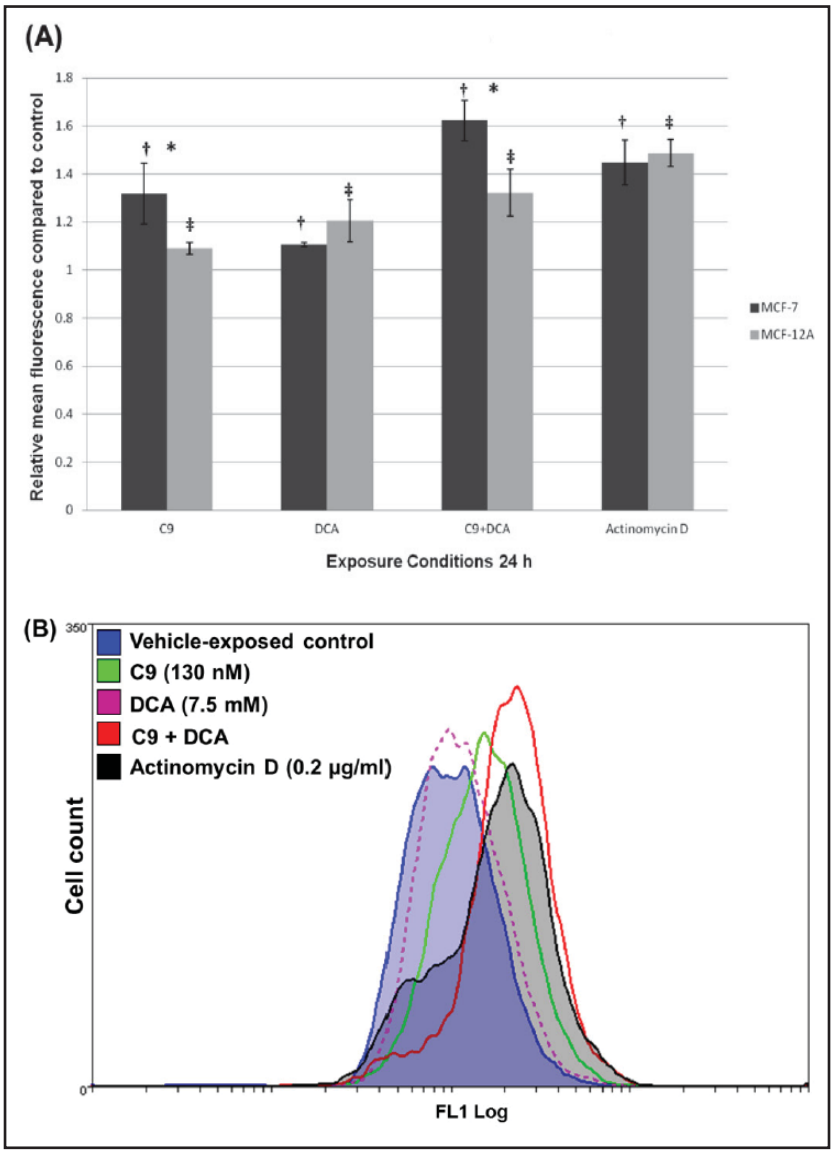


**Fig. 10.** Apoptotic-related quantification of cleaved executioner caspase 7 expression in MCF-7 and MCF-12A cells. Caspase 7 expression in treated and untreated MCF-7 and MCF-12A cells (A), as well as one representative MCF-7 data of FL1 log against cell count (B). Caspase 7 protein expression was elevated in C9-, and C9+DCA-exposed (24 h) MCF-7 cells. Caspase 7 levels also increased in C9+DCA-treated (24 h) MCF-12A cells. Differences between the active caspase 7 expression level in C9+DCA-treted MCF-7 and MCF-12A cells were statistically significant ($P < 0.05$). †, ‡, $P$-value < 0.05 after comparison of exposed cells and controls within the same cell line. *, $P$-value < 0.05 when MCF-7 and MCF-12A cells were compared for the same treatment. Actinomycin D (0.2 µg/ml) was used as a positive control for apoptosis induction.

followed for flow cytometry analysis. Fig. 10A and 10B displayed elevated caspase 7 protein expression in C9-, and C9+DCA-exposed (24 h) MCF-7 and MCF-12A cells. Caspase 7 levels increased statistically significantly in C9+DCA-treated (24 h) MCF-12A cells ($P < 0.05$).

*Autophagic activity: Transmission electron microscopy and LC3-II expression*

The present study demonstrated statistically significant decreases in cell viability in C9+DCA-treated MCF-7 cells when compared to the vehicle-exposed control. Our previous study identified statistically significant increases in early stages of apoptosis, but not late stages of apoptosis in C9+DCA-treated MCF-7 cells [9]. This result indicates that cell membranes of C9+DCA-treated MCF-7 cells are still largely intact after 24 h exposure even after the activation of mitochondrial membrane depolarisation and caspases 7 activation. This result indicated that a protective mechanism might be activated by C9+DCA after 24 h exposure. Autophagy can be induced via ROS-JNK signalling and it can play a protective role against the induction of apoptosis phenomenon [60, 61]. Since our results have identified ROS and JNK as important mediators of apoptosis in C9+DCA-treated cells, it was decided to investigate whether autophagy was also induced and whether this may explain the apparent protective effect against late stages of apoptosis.

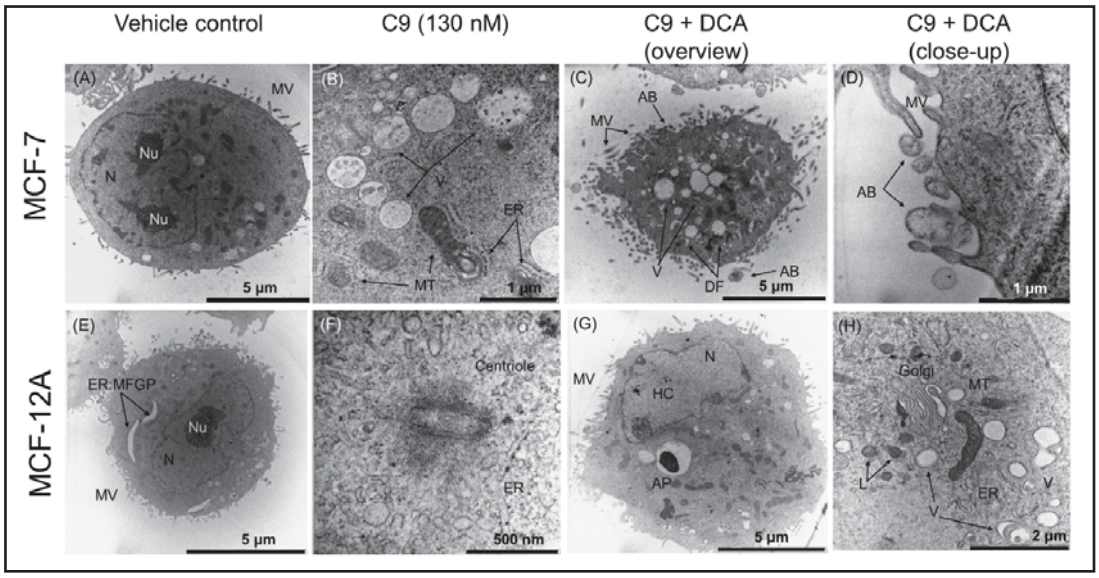


**Fig. 11.** Transmission electron micrographs of MCF-7 cells compared to MCF-12A cells after 24 h exposure to different conditions. Transmission electron micrographs of MCF-7 cells (top roll, images A-D) compared to MCF-12A cells (bottom roll, images E-H) after 24 h exposure to different conditions. Vehicle-exposed cells (A and E) showed smooth cell membrane with limited apical microvilli surround the cells. C9 (130 nM)-exposed MCF-7 (B) cells exhibited formation of vacuoles, however, large number of MCF-12A cells remain unaffected and standard cell proliferation followed after treatment. Cell exposed to C9 in combination with DCA (7.5 mM) (C, D, G and H) showed significant amount of microvilli increase, distorted cell shapes, enlarged mitochondrion, increased number of vacuoles (autophagosome and lysosomes) formation and DNA damage (heterochromatin and DNA fragmentation). Key to Fig. 11: N: Nucleus, Nu: Nucleoli, HC: Heterochromatin, MV: Apical Microvilli, AB: Apoptotic Bodies, DF: DNA Fragmentation, V: Vacuoles, MT: Mitochondrial, ER: Endoplasmic Reticulum, C: Centriole, MFGP: specialized ER for the production of human mammary milk fat globule protein, Golgi: Golgi apparatus, AP: Autophagosome and L: Lysosome.

TEM was employed to investigate ultrastructural morphology. Normal nuclear and cytoplasmic physiology was observed in vehicle-exposed MCF-7- and MCF-12A cells (Fig. 11A and 11E). Untreated control cells were round with a smooth cell membrane and a limited number of apical microvilli protrusions (Fig. 11A and 11E). Furthermore, the nucleus presented an indentation and contained one or two prominent nucleoli (Fig. 11A and 11E). The cytoplasm possessed increased quantities of mitochondria and endoplasmic reticulum. An extensive network of Golgi apparatus, centriole and specialized endoplasmic reticulum (ER) for the production of human mammary milk fat globule protein (MFGP) were also observed in untreated MCF-7- and MCF-12A cells (Fig. 11A and 11E). TEM micrographs did not illustrate stress caused by DCA treatment in both cell lines compared to controls (data not shown). Compromised cell density, endosomes, metaphase chromatid formation and autophagosomes were observed in MCF-7 cells treated with C9 (Fig. 11B). In contrast, MCF-12A cells affected by the anti-mitotic C9 (130 nM) were limited (Fig. 11F). The ordinary appearance of a pair of centrioles was spotted in MCF-12A cells after C9 treatment, indicating occurrences of regular cell division (Fig. 11F). Combination of C9+DCA-exposed MCF-7 cells displayed a distorted cell shape, a high density of digit-like apical microvilli, formations of vacuoles, lysosomes and apoptotic bodies, highly condensed chromatin (heterochromatin), as well as fragmented DNA compared to the control (Fig. 11C and 11D). The above-mentioned characteristics were also observed in MCF-12A cells treated with combination therapy (Fig. 11G and 11H). However, the intensity was in moderation compared to MCF-7 cells (Fig. 11G and 11H).

The microtubule-associated protein 1 light chain 3 (LC3) is a mammalian protein that stably associates with autophagosome membranes. LC3-I is cytosolic and LC3-II is membrane-

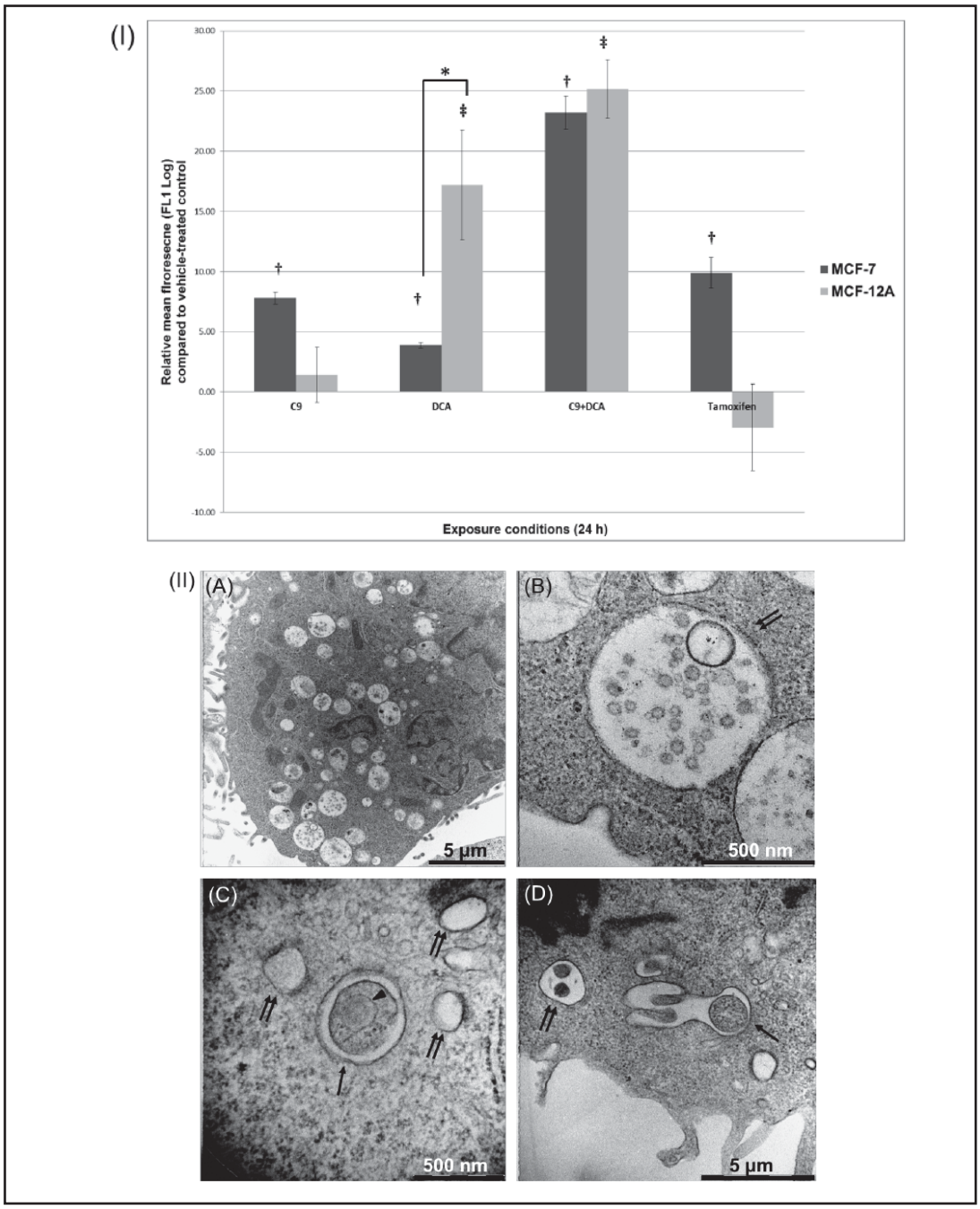


**Fig. 12.** Autophagic related quantification of specific microtubule-associated protein 1 light chain 3 II (LC3 II) expression in MCF-7 and MCF-12A cells (I) and autophagosome morphology (II). Electron microscopic analysis of C9+DCA treated MCF-7 (A and B) and MCF-12A cells (C and D). Arrows indicate autophagosomes and double arrows indicate autolysosomes/amphisomes. Arrowhead indicates fragments of endoplasmic reticulum inside the autophagosome. †,‡, *P-value* < 0.05 after comparison of exposed cells and controls within the same cell line. *, *P-value* < 0.05 when MCF-7 and MCF-12A cells were compared for the same treatment.

bound in autophagosome and thus can be used for the identification and quantification of cells undergoing autophagic processes. C9+DCA-treated MCF-7 and MCF-12A cells after 24 h exposures showed statistically significant increases (23.2% and 25.8% respectively) in LC3-II expression when compared to the vehicle-exposed control, as well as C9-treated samples

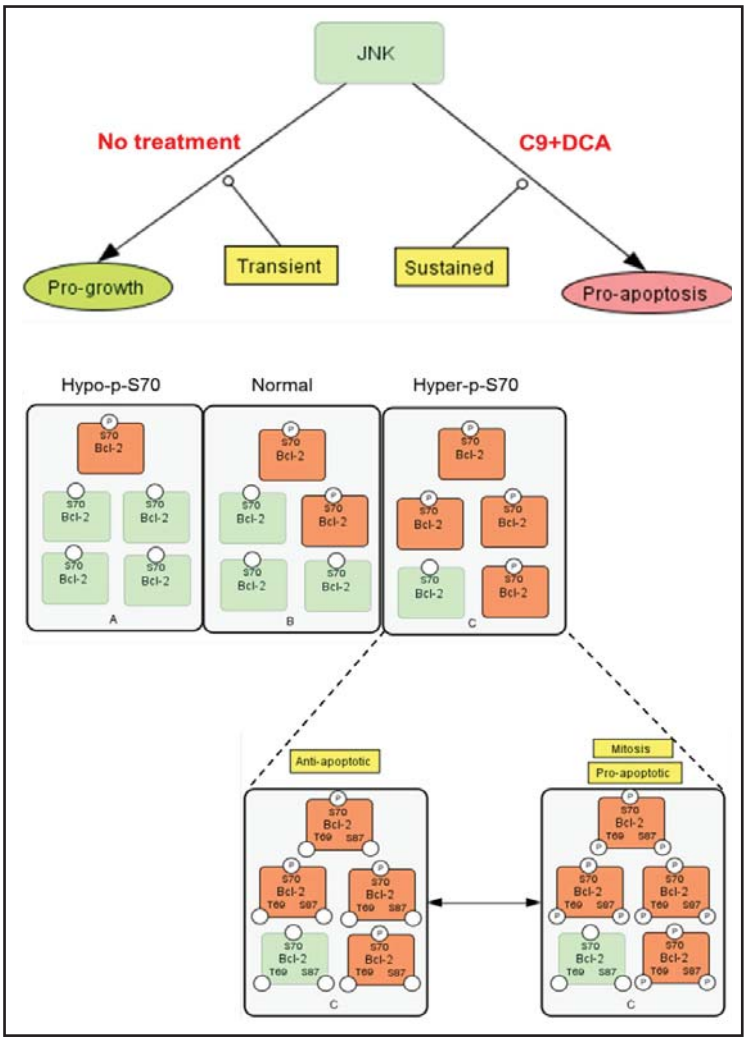


**Fig. 13.** Biphasic time-dependent activation of *c*-Jun N-terminal kinase pathway (top) and implication of phosphorylation status of the cell concerning the Bcl-2 serine 70 position (bottom). Untreated cells use transient activation of JNK pathway to promote cell growth. The combination treatment C9+DCA caused sustained activation of JNK pathway by subsequently switching on the apoptotic pathway. Three sub-populations of cells were identified signifying different protein expression levels of $Ser^{70}$ phosphorylated Bcl-2, namely, 'hypo-phosphorylation' (Hypo-p-S70), 'normal' and 'hyper-phosphorylation' (Hyper-p-S70). Bcl-2 multi-site hyper-phosphorylation (serine 70, tryptophan 69 and serine 87) and Bcl-2 serine 70 hypo-phosphorylation are associated with its pro-apoptotic properties.

($P < 0.05$) (Fig. 12 (I)). Tamoxifen (2.5 μM) was used as a positive control for autophagy induction in breast cancer cells. This finding suggests the autophagic induction is increased as a result of the combination treatment and this result supports the previously displayed TEM micrographs (Fig. 12 (II) A-D). Furthermore, several autophagic-related structures were identified within the cells that had been treated with the combination treatment. These autophagic-related structures include autophagosomes, multivascular endosomes, amphisomes, lysosomes and autolysosomes (Fig. 12 (II) A-D). Together, these results suggest that autophagy is indeed up regulated in C9+DCA-treated cells and this may explain the apparent protective effect against late stages of apoptosis after 24 h exposure.

## Discussion

The present study demonstrates that 130 nM of C9 in combination with 7.5 mM of DCA decreases cell viability in MCF-7 cells in a more pronounced way than when compared to the non-tumorigenic MCF-12A cells. Together with our previous results [9], this study has indicated that 24 h treatment of C9+DCA caused cellular stress and autophagy which was initially activated as a protective mechanism. The non-tumorigenic MCF-12A cells with healthy mitochondria function and ROS scavenge systems in place could control the treatment-induced stress when compared to MCF-7 cells. The tumorigenic cells, probably have abnormal mitochondria functions, could not recuperate from the treatment stress and

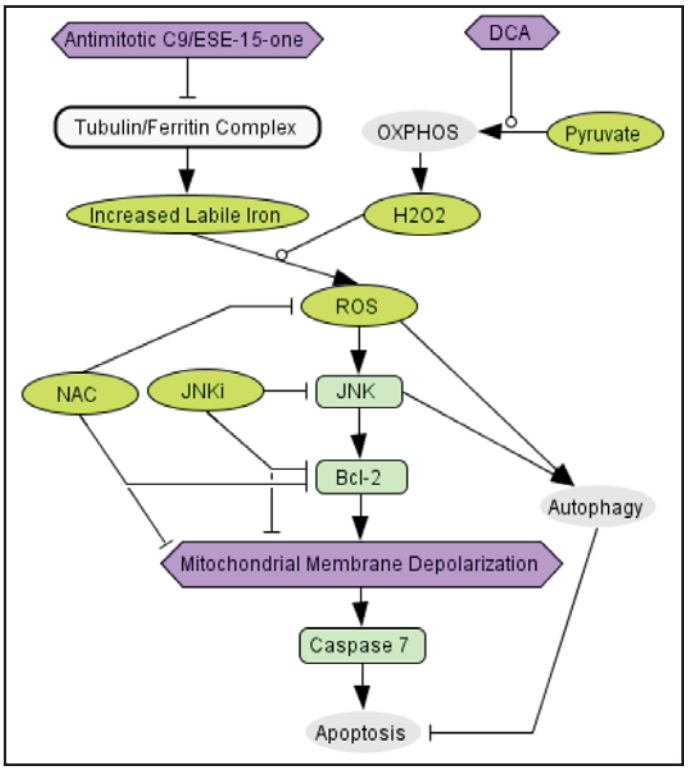


**Fig. 14.** Proposed mechanism of action of C9/ESE-15-one in combination with DCA on MCF-7 cells. C9+DCA combination treatment increases the formation of ROS which in turn activates JNK, phosphorylating Bcl-2 and results in mitochondrial-mediated induction of caspase 7 activity. Both inhibition of ROS formation (via NAC treatment) and inhibition of JNK resulted in abrogating the pro-apoptotic effects of C9+DCA. Formation of ROS and JNK activity by C9+DCA treatment can also induce an initial protective effect via autophagy that inhibits late apoptotic events.

caused apoptosis using the ROS-JNK-Bcl-2 signalling pathways. The gene expression study provided valuable information about the mechanism of action. Genes associated with cell death, as well as redox- and iron-sensitive genes implicated apoptosis and redox signalling as a possible mechanism of growth inhibition due to C9+DCA exposure.

Previous results showed lack of propidium iodide staining of the nucleus in C9+DCA-treated (24 h) cells indicated that necrotic processes were not induced in both cell lines. Moreover, apoptosis assays displayed only slight increases in the late apoptotic stages after exposure [9]. These results support the statistically significant difference observed in LDH cell viability assay after 24 h exposure in the current study. It would also suggest that the more pronounced selectivity that was observed in cell growth assays and light microscopy micrographs is more likely due to the combination treatment having a negative effect on cell proliferation rather than increased induction of late stages of apoptosis. A possible reason for this lack of increased induction of late stages of apoptosis may in part be explained by the increase in autophagic activity that was observed after 24 h treatment. Autophagy is known to have a protective effect for cancer cells under various stress situations and in this may be another example of this phenomenon [60, 61].

C9-exposed MCF-7 cells showed characteristics of compromised cell density and signs of $G_2$/M cell cycle arrest via light microscopy. Compromised cell density, $G_2$/M cell cycle arrest, membrane blebbing and formation of apoptotic bodies were observed in both cell lines after C9+DCA treatment for 24 h compared to controls. Confocal micrographs demonstrated that the mitotic spindle integrity was compromised after treatment with C9+DCA. Cells that divided in the presence of the C9+DCA treatment proceeded from being arrested at the mitotic phase to forming multiple micronuclei and apoptotic bodies. Other studies recently conducted also showed similar results where a sulphamoylated antimitotic compound-treated MCF-7, and/or MDA-MB-231 or esophageal carcinoma cells (SNO) cells showed a decrease in cell density along with morphological indicators of apoptosis [8, 28, 62]. Distorted cell shape, high density of digit-like apical microvilli, formations of vacuoles, lysosomes and apoptotic bodies, heterochromatin, as well as fragmented DNA were detected in both cell lines by means of transmission electron microscopy. This observation

is supported by a study where 17β estradiol analog-treated MDA-MB-231, MCF-7 and MCF-12A cells demonstrated the presence of apoptotic bodies and vacuoles [63]. Fragmented nuclei and apoptotic bodies were detected within tumorigenic cells that were exposed to combination compounds, which indicate late stages of apoptosis and also support previous cell cycle- and apoptotic quantification [28, 62].

Cancer cells take advantage of the autophagic process and may utilize the autophagic process to survive in hostile environments [60]. LC3-II autophagic protein expression increased in both cell lines when treated with C9+DCA for 24 h. A possible explanation for this observation is that both MCF-7 and MCF-12A use autophagy as protective pathway for survival. Several autophagic-related structures were identified which include the autophagosome, multi-vesicular endosome, amphisome, lysosome and autolysosomes within the cells that have been treated with the combination treatment. In addition, the gene expression profile demonstrated that the *SMOX* gene, which encodes protein spermine oxidase, was induced in MCF-12A cells. Spermine oxidase catalyzes the conversion of spermine to spermidine [64]. The latter process has been proven to prolong the life span of several model organisms via the induction of autophagic processes, while retarding necrotic cell death [64]. The autophagic process often occurs upstream of apoptosis [65] or inhibits apoptosis [61] to provide cells with a protective function. During stress situations, autophagy functions as a pro-survival mechanism to support the cell with essential nutrients [61]. Our present cell viability tests, equal levels of LC3-II autophagic protein expression, as well as previous apoptosis assays and data from fluorescent morphology studies [9] all support the conclusion that autophagy plays a protective role after C9+DCA treatment in MCF-7 and MCF-12A cells.

One of the most important downstream key players for the activation of the apoptotic intrinsic pathway including the disruption of the mitochondrial transmembrane potential [66]. Our current study has demonstrated that C9- and C9+DCA treatment reduced the mitochondrial potential of MCF-7 cells and not in MCF-12A cells. The reduced ΔΨm was inhibited by the broad spectrum of ROS inhibitor NAC. This result demonstrated that C9+DCA induced apoptosis via the intrinsic pathway through the production of ROS. Data from our laboratory showed that C19 (200 nM) and C10 (50 nM) caused the mitochondrial membrane potential depolarization in MCF-7 and MDA-MB-231 cancer cell lines [10, 30]. Sun et al. (on arsenic trioxide and DCA) and Shen et al. (on sorafenib and DCA) demonstrated that a combination of dichloroacetate with another chemotherapeutic agents induced apoptosis by reduced mitochondrial ΔΨm and the production of ROS in breast cancer cells and hepatocellular carcinoma respectively [67, 68]. The reason that we only observed MCF-7 cell reduced its ΔΨm, but not the MCF-12A cells after treatment was probably owing to their normal OXPHOS function [69].

The DCF-dependent fluorescence test was used to reflect the source of redox stress [36]. The DCF signal amplification is directly related to the relocation of lysosomal iron and/or mitochondrial cytochrome *c* to the cytosol [36]. The relocation of these membrane-enclosed materials (iron and cytochrome *c*) is largely caused by the organelle membrane integrity being compromised [36]. Our DCF test result suggests that treatments with DCA, C9 and C9+DCA are able to induce lysosomal rupture and/or mitochondrial damage in tumorigenic MCF-7 cells. As a consequence, large quantities of $H_2O_2$, $Fe^{2+}$ and cytochrome *c* were released into the cytosol. When a broad-spectrum ROS inhibitor NAC and ferric iron chelator deferoxamine were added in conjunction with the C9+DCA treatment, both NAC and DFO attenuated the drug's effect on MCF-7 cells in terms of mitochondrial membrane depolarization. This result confirmed that ROS, as well as $Fe^{2+}$ play an important role in apoptosis induction via mitochondrial membrane depolarization.

Acidic lysosomes function as degradative machinery for the ingestion and digestion of autophagic and heterophagic materials [50]. As a result, lysosomes contain much higher quantities of iron in a low-mass redox-active form when compared to other organelles [50, 51]. In normal cells, lysosomes utilize the iron-binding proteins, such as apoferritin, ferritin, metallothioneins and heat shock protein of 70 kDa (HSP70) to reduce tension exerted by free

Fe (II) before the protein-degradation process occurs [50, 51]. The microtubule structures are responsible for the transportation of ferritin (as oligomers) *in vitro* and *in vivo* [70]. Inhibitors of microtubule polymerization are known to lead to changes in iron metabolism including increases in ferrous iron and this change, in turn, contributes towards increased ROS formation [70]. The combination treatment, especially with C9 being an antimitotic agent, likely disturbed the distribution and transport of ferritin and thus contributed towards a higher concentration of ferritin within the cytosol. The results suggest that the mechanism of action of compound C9 and C9+DCA on tumorigenic cells and the treatment's ability to increase ROS are likely linked to its antimitotic property of targeting microtubules.

It is well-recognised that excessive ROS act as signals for the activation of stress-related JNK and/or p38 pathways [71, 72]. JNK inhibition results demonstrated that cell proliferation was decreased in untreated cells and increased in C9+DCA-treated- compared to DMSO-exposed controls. One explanation for this phenomenon is that transient JNK activation stimulated cell survival and growth, while sustained activation of JNK pathway by combination treatment motivated apoptotic signalling (Fig. 13). This proposed mechanistic theory was previously tested by Ventura et al. where the authors tested the signal transduction of JNK and demonstrated that JNK activation can have a biphasic effect [73]. Weston and Davis mention the possibility of this theory with regards to the JNK signal transduction pathway [74]. Lee et al. [75] demonstrated that JNK basal activity is indispensable for normal cell cycle progression and loss of JNK activity induces permanent cell cycle arrest following the inhibition of Bcl-2 phosphorylation and the generation of ROS. It is therefore suggested that the combination treatment of C9+DCA resulted in a sustained activation of the JNK pathway due to ROS signalling and subsequent induction of cell death.

JNK-mediated Bcl-2 multi-site phosphorylation of the non-structured loop at residues $Thr^{69}$, $Ser^{70}$ and $Ser^{87}$ was shown to interfere with its binding to pro-apoptotic, as well as, pro-autophagic BH3 domain-containing proteins [76, 77]. In response to a variety of extracellular stimuli, Bcl-2 releases pro-apoptotic factors such as Bax, in this way diminishing its inhibitory action and enabling Bax oligomerization on the mitochondrial membrane [37]. Bcl-2/Bax heterodimerization is not sufficient for full Bcl-2 anti-apoptotic function. Phosphorylation of Bcl-2 serine 70 ($Ser^{70}$) is a crucial requirement which completes its death-suppressor signalling activity [39]. Hypo-phosphorylation/dephosphorylation at $Ser^{70}$ is associated with apoptosis induction through the mitochondrial pathway [40]. Bcl-2 $Ser^{70}$ hyper-phosphorylation is required for Bcl-2's full and potent anti-apoptotic function [78].

Treatment C9+DCA disturbed the Bcl-2 phosphorylation status ($Ser^{70}$) of both MCF-7 and MCF-12A cells with an increase in both hypo- and hyper-phosphorylated Bcl-2 (Fig. 13). Our study result suggests that treatment C9 and C9+DCA has the ability to activate anti-apoptotic Bcl-2 protein in MCF-7 cells at the post-translational level of phosphorylation. Bcl-2 $Ser^{70}$ hypo-phosphorylation is related to the intrinsic mitochondrial pathway of apoptosis induction; thus, treatment of C9 or C9+DCA possibly induced apoptosis of MCF-7 cells through the intrinsic pathway.

Treatments of C9 or C9+DCA on MCF-7 cells also induced Bcl-2 $Ser^{70}$ hyper-phosphorylation. An increase in $Ser^{70}$, $Trp^{69}$ and $Ser^{87}$ multi-site phosphorylation is associated with apoptosis induction and is related to drugs causing $G_2$/M arrest in MCF-7 cells [40]. This study's results are consistent with research conducted by Haldar et al. who showed that the spindle poison/antimitotic compounds induced cancer cell death through phosphorylation of Bcl-2 [77, 79]. Previous MitoCapture™ and DCF-test results demonstrated that treatments with C9- or C9+DCA against MCF-7 cells caused $\Delta\Psi m$ depolarization as well as possible ROS formation. Together with the Bcl-2 results, it is therefore argued that Bcl-2 multi-site phosphorylation ($Ser^{70}$, $Trp^{69}$ and $Ser^{87}$) might be induced by treatment with C9 and C9+DCA in MCF-7 cells (Fig. 13). Furthermore, our results also demonstrated that the addition of DCA sensitised C9 towards MCF-7 cells in terms of Bcl-2 phosphorylation status. This observation can be attributed to DCA causing a substantial amount of ROS formation, which served as a signal to stimulate the MAPK pathway and subsequently activate Bcl-2 phosphorylation [80].

## Conclusion

Cancer cells tend to have an increased pro-oxidant status and an intracellular pro-oxidant status above a certain level selectively activates pro-apoptotic stress-activated protein kinases (SAPK) pathways [81]. The source of the increase in ROS may be two-fold (Fig. 14). Firstly, inhibitors of microtubule polymerization are known to lead to changes in iron metabolism, leading to increases in ferrous iron and this in turn contributes towards increased ROS formation [70]. Malignant cells such as MCF-7, cells when compared to MCF-12A cells, may be more sensitive towards iron-mediated cell death induction by antimitotics as been demonstrated that increased intracellular ferritin is found in malignant breast cancer cells [10, 82, 83]. Secondly, DCA treatment is known to induce the production of ROS in cancer cells by promoting oxidative phosphorylation [18] (Fig. 14).

In conclusion, the combination of these two compounds may thus work synergistically to take advantage of the pro-oxidant status of cancer cells and to induce production of ROS above a certain threshold level, leading to the selective activation of SAPKs and cell death (Fig. 14). Results obtained contribute to elucidate the functional roles of the pathways involved in selectively killing off cancer cells by a glycolytic inhibitor and an antimitotic compound. This study is the first to elucidate the mechanism of action of the antimitotic C9 in combination with the glycolytic inhibitor DCA with the involvement of ROS, JNK and Bcl-2 signalling pathway *in vitro*. This project warrants further research to develop viable and functional combination treatments as clinically useable anticancer agents.

## Acknowledgements

A Hall and C van der Merwe (Laboratory for Microscopy and Microanalysis, University of Pretoria (UP)) for technical assistance. B English (UP: Faculty of Health Sciences Research Office) for editing the manuscript. Professors P Becker (Medical Research Council of South Africa) and F Joubert (Bioinformatics Unit, UP) for statistical consultations. This research project was supported by grants from the Medical Research Council of South Africa (AL343, AOW110), the Cancer Association of South Africa (AS201, AOV741, AOW228), the National Research Foundation (NRF) (AL239, N00591), RESCOM School of Medicine of the University of Pretoria and the Struwig-Germeshuysen Cancer Research Trust of South Africa (AN074). Flow cytometric analyses were performed at the Department of Pharmacology, Faculty of Health Sciences, University of Pretoria (Pretoria, South Africa). Transmission Electron Microscopy was conducted at the Electron Microscopy Unit of University of Pretoria (Pretoria, South Africa).

## Disclosure Statement

The authors declare that they have no competing interests.

## References

1 Attolini CS, Michor F: Evolutionary theory of cancer. Ann N Y Acad Sci 2009;1168:23-51.
2 Hanahan D, Weinberg RA: The hallmarks of cancer. Cell 2000;100:57-70.
3 Hanahan D, Weinberg RA: Hallmarks of cancer: the next generation. Cell 2011;144:646-674.
4 Diaz LA, Jr, Williams RT, Wu J, Kinde I, Hecht JR, Berlin J, Allen B, Bozic I, Reiter JG, Nowak MA, Kinzler KW, Oliner KS, Vogelstein B: The molecular evolution of acquired resistance to targeted EGFR blockade in colorectal cancers. Nature 2012;486:537-540.
5 Vander Heiden MG, Cantley LC, Thompson CB: Understanding the Warburg effect: the metabolic requirements of cell proliferation. Science 2009;324:1029-1033.
6 Raez LE, Papadopoulos K, Ricart AD, Chiorean EG, Dipaola RS, Stein MN, Rocha Lima CM, Schlesselman JJ, Tolba K, Langmuir VK, Kroll S, Jung DT, Kurtoglu M, Rosenblatt J, Lampidis TJ: A phase I dose-escalation trial of 2-deoxy-D-glucose alone or combined with docetaxel in patients with advanced solid tumors. Cancer Chemother Pharmacol 2013;71:523-530.

7 Tagg SL, Foster PA, Leese MP, Potter BV, Reed MJ, Purohit A, Newman SP: 2-Methoxyoestradiol-3,17-O,O-bis-sulphamate and 2-deoxy-D-glucose in combination: a potential treatment for breast and prostate cancer. Br J Cancer 2008;99:1842-1848.
8 Stander A, Joubert F, Joubert A: Docking, synthesis, and in vitro evaluation of antimitotic estrone analogs. Chem Biol Drug Des 2011;77:173-181.
9 Stander XX, Stander BA, Joubert AM: In vitro effects of an in silico-modelled 17beta-estradiol derivative in combination with dichloroacetic acid on MCF-7 and MCF-12A cells. Cell Prolif 2011;44:567-581.
10 Stander BA, Joubert F, Tu C, Sippel KH, McKenna R, Joubert AM: Signaling Pathways of ESE-16, an Antimitotic and Anticarbonic Anhydrase Estradiol Analog, in Breast Cancer Cells. PLoS One 2013;8:e53853.
11 Supuran CT, Scozzafava A: Carbonic anhydrases as targets for medicinal chemistry. Bioorg Med Chem 2007;15:4336-4350.
12 Cushman M, He HM, Katzenellenbogen JA, Lin CM, Hamel E: Synthesis, antitubulin and antimitotic activity, and cytotoxicity of analogs of 2-methoxyestradiol, an endogenous mammalian metabolite of estradiol that inhibits tubulin polymerization by binding to the colchicine binding site. J Med Chem 1995;38:2041-2049.
13 Tinley TL, Leal RM, Randall-Hlubek DA, Cessac JW, Wilkens LR, Rao PN, Mooberry SL: Novel 2-methoxyestradiol analogues with antitumor activity. Cancer Res 2003;63:1538-1549.
14 Knoechel TR, Tucker AD, Robinson CM, Phillips C, Taylor W, Bungay PJ, Kasten SA, Roche TE, Brown DG: Regulatory roles of the N-terminal domain based on crystal structures of human pyruvate dehydrogenase kinase 2 containing physiological and synthetic ligands. Biochemistry 2006;45:402-415.
15 Garber K: Energy deregulation: licensing tumors to grow. Science 2006;312:1158-1159.
16 Ristow M: Oxidative metabolism in cancer growth. Curr Opin Clin Nutr Metab Care 2006;9:339-345.
17 Schulz TJ, Thierbach R, Voigt A, Drewes G, Mietzner B, Steinberg P, Pfeiffer AF, Ristow M: Induction of oxidative metabolism by mitochondrial frataxin inhibits cancer growth: Otto Warburg revisited. J Biol Chem 2006;281:977-981.
18 Bonnet S, Archer SL, Allalunis-Turner J, Haromy A, Beaulieu C, Thompson R, Lee CT, Lopaschuk GD, Puttagunta L, Bonnet S, Harry G, Hashimoto K, Porter CJ, Andrade MA, Thebaud B, Michelakis ED: A mitochondria-K+ channel axis is suppressed in cancer and its normalization promotes apoptosis and inhibits cancer growth. Cancer Cell 2007;11:37-51.
19 Gatenby RA, Gillies RJ: Why do cancers have high aerobic glycolysis? Nat Rev Cancer 2004;4:891-899.
20 Michelakis E, Sutendra G, Dromparis P, Webster L, Haromy A, Niven E, Maguire C, Gammer T, Mackey J, Fulton D: Metabolic modulation of glioblastoma with dichloroacetate. Sci Transl Med 2010;2:31ra34.
21 Sutendra G, Dromparis P, Kinnaird A, Stenson T, Haromy A, Parker J, McMurtry M, Michelakis E: Mitochondrial activation by inhibition of PDKII suppresses HIF1a signaling and angiogenesis in cancer. Oncogene 2013;32:1638-1650.
22 Seth P, Grant A, Tang J, Vinogradov E, Wang X, Lenkinski R, Sukhatme VP: On-target inhibition of tumor fermentative glycolysis as visualized by hyperpolarized pyruvate. Neoplasia 2011;13:60-71.
23 Chou TC: Drug combination studies and their synergy quantification using the Chou-Talalay method. Cancer Res 2010;70:440-446.
24 Goldin A, Venditti JM, Mantel N, Kline I, Gang M: Evaluation of combination chemotherapy with three drugs. Cancer Res 1968;28:950-960.
25 Garbutcheon-Singh KB, Harper BW, Myers S, Aldrich-Wright JR: Combination studies of platinum(II)-based metallointercalators with buthionine-S,R-sulfoximine, 3-bromopyruvate, cisplatin or carboplatin. Metallomics 2014;6:126-131.
26 Allen M, Millett P, Dawes E, Rushton N: Lactate dehydrogenase activity as a rapid and sensitive test for the quantification of cell numbers in vitro. Clin Mater 1994;16:189-194.
27 Fischer A, Jacobson K, Rose J, Zeller R: Preparation of cells and tissues for fluorescence microscopy. In: Goldman SA, (ed): Basic Methods in Microscopy Cold Spring Harbor, NY, USA., Cold Spring Harbor Laboratory Press, 2006.
28 Visagie M, Mqoco T, Joubert A: Sulphamoylated estradiol analogue induces antiproliferative activity and apoptosis in breast cell lines. Cell Mol Biol Lett 2012;17:549-558.
29 Visagie MH, Joubert AM: The in vitro effects of 2-methoxyestradiol-bis-sulphamate on cell numbers, membrane integrity and cell morphology, and the possible induction of apoptosis and autophagy in a non-tumorigenic breast epithelial cell line. Cell Mol Biol Lett 2010;15:564-581.

30 Stander BA, Joubert F, Tu C, Sippel KH, McKenna R, Joubert AM: In Vitro Evaluation of ESE-15-ol, an Estradiol Analogue with Nanomolar Antimitotic and Carbonic Anhydrase Inhibitory Activity. PLoS One 2012;7:e52205.
31 Stander BA, Marais S, Vorster CJ, Joubert AM: In vitro effects of 2-methoxyestradiol on morphology, cell cycle progression, cell death and gene expression changes in the tumorigenic MCF-7 breast epithelial cell line. J Steroid Biochem Mol Biol 2010;119:149-160.
32 Wettenhall JM, Smyth GK: limmaGUI: a graphical user interface for linear modeling of microarray data. Bioinformatics 2004;20:3705-3706.
33 Smyth G: Limma: linear models for microarray data. Bioinformatics and computational biology solutions using R and bioconductor. Springer, 2005, pp 397-420.
34 Pirooznia M, Nagarajan V, Deng Y: GeneVenn—a web application for comparing gene lists using Venn diagrams. Bioinformation 2007;1:420-422.
35 Tabas-Madrid D, Nogales-Cadenas R, Pascual-Montano A: GeneCodis3: a non-redundant and modular enrichment analysis tool for functional genomics. Nucleic Acids Res 2012;40(Web Server issue):W478-483.
36 Karlsson M, Kurz T, Brunk UT, Nilsson SE, Frennesson CI: What does the commonly used DCF test for oxidative stress really show? Biochem J 2010;428:183-190.
37 Berridge MJ: Cell Signalling Biology. Portland Press Ltd. 2012.
38 Letai AG: Diagnosing and exploiting cancer's addiction to blocks in apoptosis. Nat Rev Cancer 2008;8121-132.
39 Ito T, Deng X, Carr B, May WS: Bcl-2 phosphorylation required for anti-apoptosis function. J Biol Chem 1997;272:11671-11673.
40 Letai A, Kutuk O: Regulation of Bcl-2 family proteins by posttranslational modifications. Curr Mol Med 2008;8:102-118.
41 Spencer JP: The interactions of flavonoids within neuronal signalling pathways. Genes Nutr 2007;2:257-273.
42 Passiatore G, Gentilella A, Rom S, Pacifici M, Bergonzini V, Peruzzi F: Induction of Id-1 by FGF-2 involves activity of EGR-1 and sensitizes neuroblastoma cells to cell death. J Cell Physiol 2011;226:1763-1770.
43 Graziano MJ, Spoon TA, Cockrell EA, Rowse PE, Gonzales AJ: Induction of Apoptosis in Rat Peripheral Blood Lymphocytes by the Anticancer Drug CI-994 (Acetyldinaline)(*). J Biomed Biotechnol 2001;1:52-61.
44 Parhamifar L, Andersen H, Moghimi SM: Lactate dehydrogenase assay for assessment of polycation cytotoxicity. In: Nanotechnology for Nucleic Acid Delivery: Springer, 2013, pp 13-22.
45 Roy G, De Crescenzo G, Khaleghpour K, Kahvejian A, O'Connor-McCourt M, Sonenberg N: Paip1 interacts with poly(A) binding protein through two independent binding motifs. Mol Cell Biol 2002;22:3769-3782.
46 Imataka H, Sonenberg N: Human eukaryotic translation initiation factor 4G (eIF4G) possesses two separate and independent binding sites for eIF4A. Mol Cell Biol 1997;17:6940-6947.
47 Cao Y, Karin M: NF-kappaB in mammary gland development and breast cancer. J Mammary Gland Biol Neoplasia 2003;8:215-223.
48 Murata K, Hattori M, Hirai N, Shinozuka Y, Hirata H, Kageyama R, Sakai T, Minato N: Hes1 directly controls cell proliferation through the transcriptional repression of p27Kip1. Mol Cell Biol 2005;25:4262-4271.
49 Fu T-J, Peng J, Lee G, Price DH, Flores O: Cyclin K functions as a CDK9 regulatory subunit and participates in RNA polymerase II transcription. J Biol Chem 1999;274:34527-34530.
50 Terman A, Kurz T: Lysosomal iron, iron chelation, and cell death. Antioxid Redox Signal 2013;18:888-898.
51 Kurz T, Eaton JW, Brunk UT: The role of lysosomes in iron metabolism and recycling. Int J Biochem Cell Biol 2011;43:1686-1697.
52 Luo Y, Kong F, Wang Z, Chen D, Liu Q, Wang T, Xu R, Wang X, Yang JY: Loss of ASAP3 destabilizes cytoskeletal protein ACTG1 to suppress cancer cell migration. Mol Med Rep 2014;9:387-394.
53 Goswami C, Hucho T: Submembraneous microtubule cytoskeleton: biochemical and functional interplay of TRP channels with the cytoskeleton. FEBS J 2008;275:4684-4699.
54 Heng JI, Chariot A, Nguyen L: Molecular layers underlying cytoskeletal remodelling during cortical development. Trends Neurosci 2010;33:38-47.
55 Dean M, Fojo T, Bates S: Tumour stem cells and drug resistance. Nat Rev Cancer 2005;5:275-284.
56 Jaeger W: Classical resistance mechanisms. Int J Clin Pharmacol Ther 2009;47:46-48.
57 Liu G, Chen X: The ferredoxin reductase gene is regulated by the p53 family and sensitizes cells to oxidative stress-induced apoptosis. Oncogene 2002;21:7195-7204.

58 Imamichi Y, Mizutani T, Ju Y, Matsumura T, Kawabe S, Kanno M, Yazawa T, Miyamoto K: Transcriptional regulation of human ferredoxin reductase through an intronic enhancer in steroidogenic cells. Biochim Biophys Acta 2014;1839:33-42.
59 Valko M, Rhodes CJ, Moncol J, Izakovic M, Mazur M: Free radicals, metals and antioxidants in oxidative stress-induced cancer. Chem Biol Interact 2006;160:1-40.
60 Yang ZJ, Chee CE, Huang S, Sinicrope FA: The role of autophagy in cancer: therapeutic implications. Mol Cancer Ther 2011;10:1533-1541.
61 Platini F, Perez-Tomas R, Ambrosio S, Tessitore L: Understanding autophagy in cell death control. Curr Pharm Des 2010;16:101-113.
62 Wolmarans E, Mqoco TV, Stander A, Nkandeu SD, Sippel K, McKenna R, Joubert A: Novel estradiol analogue induces apoptosis and autophagy in esophageal carcinoma cells. Cell Mol Biol Lett 2014;19:98-115.
63 Visagie MH, Birkholtz LM, Joubert AM: 17-beta-estradiol analog inhibits cell proliferation by induction of apoptosis in breast cell lines. Microsc Res Tech 2014;77:236-242.
64 Madeo F, Eisenberg T, Buttner S, Ruckenstuhl C, Kroemer G: Spermidine: a novel autophagy inducer and longevity elixir. Autophagy 2010;6:160-162.
65 Eisenberg-Lerner A, Bialik S, Simon H, Kimchi A: Life and death partners: apoptosis, autophagy and the cross-talk between them. Cell Death Differ 2009;16:966-975.
66 Elmore S: Apoptosis: a review of programmed cell death. Toxicol Pathol 2007;35:495-516.
67 Sun RC, Board PG, Blackburn AC: Targeting metabolism with arsenic trioxide and dichloroacetate in breast cancer cells. Mol Cancer 2011;10:142.
68 Shen YC, Ou DL, Hsu C, Lin KL, Chang CY, Lin CY, Liu SH, Cheng AL: Activating oxidative phosphorylation by a pyruvate dehydrogenase kinase inhibitor overcomes sorafenib resistance of hepatocellular carcinoma. Br J Cancer 2013;108:72-81.
69 Elliott RL, Jiang XP, Head JF: Mitochondria organelle transplantation: introduction of normal epithelial mitochondria into human cancer cells inhibits proliferation and increases drug sensitivity. Breast Cancer Res Treat 2012;136:347-354.
70 Hasan MR, Koikawa S, Kotani S, Miyamoto S, Nakagawa H: Ferritin forms dynamic oligomers to associate with microtubules in vivo: implication for the role of microtubules in iron metabolism. Exp Cell Res 2006;312:1950-1960.
71 Tobiume K, Matsuzawa A, Takahashi T, Nishitoh H, Morita K, Takeda K, Minowa O, Miyazono K, Noda T, Ichijo H: ASK1 is required for sustained activations of JNK/p38 MAP kinases and apoptosis. EMBO Rep 2001;2:222-228.
72 Davis RJ: Signal transduction by the JNK group of MAP kinases. In: Gordon L, Morgan D, (eds); Inflammatory Processes: Molecular Mechanisms and Therapeutic Opportunities. Springer, 2000, pp 13-21.
73 Ventura JJ, Hubner A, Zhang C, Flavell RA, Shokat KM, Davis RJ: Chemical genetic analysis of the time course of signal transduction by JNK. Mol Cell 2006;21:701-710.
74 Weston CR, Davis RJ: The JNK signal transduction pathway. Curr Opin Cell Biol 2007;19:142-149.
75 Lee J-J, Lee J-H, Ko Y-G, Hong S, Lee J-S: Prevention of premature senescence requires JNK regulation of Bcl-2 and reactive oxygen species. Oncogene 2009;29:561-575.
76 Wei Y, Sinha S, Levine B: Dual role of JNK1-mediated phosphorylation of Bcl-2 in autophagy and apoptosis regulation. Autophagy 2008;4:949-951.
77 Haldar S, Chintapalli J, Croce CM: Taxol induces bcl-2 phosphorylation and death of prostate cancer cells. Cancer Res 1996;56:1253-1255.
78 Ruvolo PP, Deng X, May WS: Phosphorylation of Bcl2 and regulation of apoptosis. Leukemia 2001;15:515-522.
79 Haldar S, Basu A, Croce CM: Bcl2 is the guardian of microtubule integrity. Cancer Res 1997;57:229-233.
80 Li D, Ueta E, Kimura T, Yamamoto T, Osaki T: Reactive oxygen species (ROS) control the expression of Bcl-2 family proteins by regulating their phosphorylation and ubiquitination. Cancer Sci 2004;95:644-650.
81 Matsuzawa A, Ichijo H: Redox control of cell fate by MAP kinase: physiological roles of ASK1-MAP kinase pathway in stress signaling. Biochimica et Biophysica Acta 2008;1780:1325-1336.
82 Shpyleva SI, Tryndyak VP, Kovalchuk O, Starlard-Davenport A, Chekhun VF, Beland FA, Pogribny IP: Role of ferritin alterations in human breast cancer cells. Breast Cancer Res Treat 2011;126:63-71.
83 Bresgen N, Jaksch H, Lacher H, Ohlenschlager I, Uchida K, Eckl PM: Iron-mediated oxidative stress plays an essential role in ferritin-induced cell death. Free Radic Biol Med 2010;48:1347-1357.